

General Disclaimer

One or more of the Following Statements may affect this Document

- This document has been reproduced from the best copy furnished by the organizational source. It is being released in the interest of making available as much information as possible.
- This document may contain data, which exceeds the sheet parameters. It was furnished in this condition by the organizational source and is the best copy available.
- This document may contain tone-on-tone or color graphs, charts and/or pictures, which have been reproduced in black and white.
- This document is paginated as submitted by the original source.
- Portions of this document are not fully legible due to the historical nature of some of the material. However, it is the best reproduction available from the original submission.



THE PENNSYLVANIA
STATE UNIVERSITY

INVESTIGATION OF ENVIRONMENTAL PERTURBATIONS ON A PASSIVE ASYMMETRIC SATELLITE

BY
VINCENT TATE

(NASA-CF-146507) INVESTIGATION OF
ENVIRONMENTAL PERTURBATIONS ON PASSIVE
ASYMMETRIC SATELLITE (Pennsylvania State
Univ.) 73 p HC \$4.50

CSCI 22C

N76-19205

Unclas
20684

G3/15

ASTRONAUTICS RESEARCH REPORT
NO. 76-1

APRIL 1976

DEPARTMENT OF AEROSPACE ENGINEERING
UNIVERSITY PARK, PENNSYLVANIA



RESEARCH PARTIALLY SUPPORTED BY NASA
GRANTS NGR 39-009-162/NSG-7078

ACKNOWLEDGMENTS

The author wishes to acknowledge his advisor, Dr. Marshall H. Kaplan, Associate Professor of Aerospace Engineering for his assistance.

This investigation was made possible partially by the National Aeronautics and Space Administration under NASA Grants NGR 39-009-162 and NSG-7078.

TABLE OF CONTENTS

	Page
ACKNOWLEDGMENTS	ii
LIST OF FIGURES	iv
NOMENCLATURE	vi
ABSTRACT	x
I. INTRODUCTION.	1
II. COORDINATE SYSTEMS.	3
III. DYNAMIC ANALYSIS	13
IV. ENVIRONMENTAL PERTURBATION MODELS	17
Gravity-Gradient	17
Aerodynamic Drag	20
Magnetic Torque Model	26
Solar Radiation Pressure.	30
V. APPLICATION TO SKYLAB	37
VI. SIMULATION RESULTS.	38
Torque-Free Results	38
Gravity-Gradient Results.	41
Aerodynamic Drag Results.	46
Combined Effects of Gravity-Gradient and Aerodynamic Torques	52
VII. CONCLUSIONS AND RECOMMENDATIONS	57
REFERENCES	59
APPENDIX A: Initial Conditions for the Slow Tumble Mode.	61
APPENDIX B: Skylab's Aerodynamic Drag Moment Coefficients.	62
APPENDIX C: Skylab's Orbit and Satellite Parameters.	63

LIST OF FIGURES

Figure		Page
1	Geocentric Inertial Coordinate System	4
2	Geocentric Inertial and Sun Coordinate System	5
3	Inertial and Orbital Coordinate System.	6
4	Euler Rotations	11
5	Nutation and Precession Angles in the Orbit Coordinate System	15
6	Coordinate System Used in the Gravity-Gradient Torque Derivation.	18
7	Aerodynamic Moment Coefficients in Satellite Body Coordinate System	22
8	Skylab's Configuration for Aerodynamic Drag Model	25
9	Coordinate System for the Earth's Magnetic Field Model	28
10	Geometry for the Solar Radiation Physical Model	31
11	Geometry for the Shadow Model	36
12	Nutation and Precession Angles for Torque-Free Solution	39
13	Nadir Angle for Torque-Free Solution.	40
14	Nadir Angle for Gravity-Gradient.	42
15	Effect of Gravity-Gradient on the Angular Momentum and Energy.	43
16	Nutation and Precession Angles for Gravity-Gradient	45
17	Nadir Angle for Aerodynamic Drag.	47
18	Aerodynamic Drag Effect on the Angular Momentum and Energy.	48
19	Effect of Aerodynamic Drag on the Y and Z Angular Momentum Components in the Body Coordinate System.	50
20	Aerodynamic Drag Effect on the Precession and Nutation Angles.	51

LIST OF FIGURES (continued)

Figure		Page
21	Aerodynamic Drag and Gravity-Gradient Effect on the Angular Momentum and Energy.	53
22	Nadir Angle for Aerodynamic Drag and Gravity-Gradient. . .	55
23	Aerodynamic Drag and Gravity-Gradient Effect on the Precession and Nutation Angles	56

NOMENCLATURE

a	Orbit semi-major axis
A, B, C	Satellite principal moment of inertias
A_i, B_i	Fourier coefficients
A_{ref}	Skylab reference area
c_x, c_y, c_z	Skylab roll, pitch, and yaw aerodynamic drag moment coefficients
C_D	Aerodynamic drag coefficient
D	Angle between earth and sun vectors
D_{AE}	Number of days after vernal equinox
D_{ref}	Skylab reference diameter
dS	Satellite surface element
E	Angle between earth radius and orbit radius vector as shown in Figure (11)
\bar{e}_1, \bar{e}_2	Unit vectors
e_θ, e_r, e_λ	Earth magnetic force components
F_a	Aerodynamic drag force
F_G	Earth gravitational force
F	Solar radiation force
F_i	Absorbed solar radiation force components
F_r	Reflected solar radiation force components
F_s	Solar radiation force
g_N^K, h_N^K	Magnetic field spherical harmonics coefficient
GCI	Geocentric inertial coordinate system
h	Satellite angular momentum
h_x, h_y, h_z	x, y, z angular momentum components with respect to the satellite principal axes

NOMENCLATURE (continued)

i	Orbit's inclination to the equatorial plane
i_s	Inclination of ecliptic plane to earth's equatorial plane
I_{xy}, I_{yz}, I_{xz}	Satellite products of inertia
\bar{L}_S	Sun vector in geocentric inertial system
\bar{L}	Sun vector in geocentric inertial system
\bar{M}	Satellite magnetic dipole field vector
M_A	Aerodynamic moment
M_G	Gravity-gradient torque
M_m	Magnetic torque
M_S	Solar radiation torque
M_x, M_y, M_z	Moments in the satellite's coordinate system
\bar{n}	Unit vector normal to surface element
P	Orbit period
P_S	Solar radiation pressure
q	Dynamic pressure = $1/2 \rho V^2$
r	Distance from earth center to mass element dm
R	Satellite orbit radius
R_e	Earth radius
S_A	Satellite surface absorption coefficient
S_r	Satellite surface reflection coefficient
T	Satellite energy
V_o	Satellite orbital velocity
V	Satellite velocity relative to the incident stream
V_m	Earth magnetic field potential

NOMENCLATURE (continued)

X_I, Y_I, Z_I	Geocentric inertial coordinate system
X_O, Y_O, Z_O	Orbital reference coordinate system
X_G, Y_G, Z_G	Greenwich geocentric coordinate system
X_b, Y_b, Z_b	Satellite's body coordinate system
α	Satellite true anomaly
α_a	Angle of attack
β	Right ascension of the orbit ascending node
$\dot{\beta}$	Ascending nodal regression rate
$\gamma, \gamma_1, \gamma_2$	Solar reflection angles
γ_V	Angle of attack
δ	Nutation angle in orbital coordinate system
η	Nadir angle
θ_M	Satellite colatitude
θ_s	Angular displacement of the sun from vernal equinox
λ	Precession angle in orbital coordinate system
λ_o	Angular displacement of Greenwich line from vernal equinox
λ_i	Initial angle between Greenwich line and vernal equinox
λ_M	East longitude
μ	Earth's gravitational constant
ρ	Distance from satellite center of mass to mass element dm
ρ_a	Atmospheric density
ϕ_a	Roll angle
ψ, θ, ϕ	Euler's rotation angles
Ω_e	Earth rotational rate

NOMENCLATURE (continued)

ω_e	Satellite orbital rate
$\omega_x, \omega_y, \omega_z$	Satellite's body angular velocities
$\dot{\omega}_x, \dot{\omega}_y, \dot{\omega}_z$	Satellite's body angular accelerations

ABSTRACT

The effects of environmental perturbations on the attitude of a slow tumbling earth-oriented satellite are investigated. The environmental perturbations considered were aerodynamic drag, gravity-gradient, solar radiation pressure, and magnetic torques. The Euler attitude equations were solved numerically for the Skylab spacecraft. Results are presented for both torque-free motion and for cases in which aerodynamic and gravity-gradient torques are acting in a slow tumble mode. Simulations show gravity-gradient effects on satellite momentum to be cyclic and to increase the precession rate of the angular momentum vector about the radius vector. This also tends to align the minor axis along the radius vector. Aerodynamic drag initially decreases angular momentum, slowly precesses the momentum vector about the radius vector, and finally drives the satellite into an unstable mode. Combined gravity-gradient and aerodynamic torques reduce angular momentum and energy, and induce a steady precession rate of the momentum vector about the radius vector.

CHAPTER I

INTRODUCTION

With the coming of the space shuttle the opportunity for retrieving and repairing satellites will become feasible. With retrieval capability, future satellites may be designed with docking ports to be used by a retrieval device for attaching to the satellite. To design these devices and the location of docking ports on the satellite, the final attitude state of the passive satellite must be determined.

The research in this thesis involves a numerical study of the general attitude motion for an asymmetric satellite due to environmental perturbations. These perturbations included gravity-gradient, aerodynamic drag, solar radiation pressure, and magnetic torques.

The general analytic solution to Euler's moment equations are elliptical functions for the torque free case.⁽¹⁾ General solutions to Euler's equations with complicated torque functions do not exist and solutions are primarily numerical. Some solutions have been obtained by linearization for special cases. Here the equations could not be linearized to study detailed motion. However, Euler's moment equations were solved numerically using a fourth order Runge-Kutta and an Adams-Bashforth predictor-corrector integration technique. The dynamical state of interest was a slow tumble mode, defined as small angular rates about the three body axes. Initial conditions are explained in Appendix A. The satellite was considered to be a rigid body with no control system functioning.

The asymmetric satellite studied in this research was the Skylab spacecraft. Its attitude control system is assumed to be shut down.

Linearization of the equation of motion was possible in order to study stability under effects of gravity-gradient and aerodynamic drag. (2,3,4)

This stability analysis has indicated the spacecraft to be unstable in the presence of gravity-gradient with aerodynamic torques.

CHAPTER II
COORDINATE SYSTEMS

This section describes the coordinate systems used in determining the position and attitude of the satellite. The inertial coordinate system is shown in Figure 1 with its origin at the Earth's center. Z_I lies in the equatorial plane pointing in a positive direction away from the center of the earth along the vernal equinox. Y_I is perpendicular to the equatorial plane and positive northward. X_I is in a direction forming a positive right handed coordinate system. The inertial coordinate system will be denoted as

$$[\bar{L}]_I = \begin{bmatrix} \bar{X}_I \\ \bar{Y}_I \\ \bar{Z}_I \end{bmatrix} \quad (1)$$

The relationship of the apparent motion of the sun about the earth is shown in Figure 2. The unit vector from the earth to the sun in the geocentric inertial coordinate system is

$$\bar{L}_s = \sin \theta_s \cos i_s \bar{i}_I + \sin \theta_s \sin i_s \bar{j}_I + \cos \theta_s \bar{k}_I \quad (2)$$

where

$$\theta_s = \frac{360}{365.24} D_{AE} \quad (3)$$

D_{AE} is the number of days after vernal equinox. i_s is the inclination of the ecliptic plane to the equatorial plane of the earth (obliquity of the ecliptic).

The relationship between the orbital and inertial coordinate system is shown in Figure 3. The transformation from inertial to orbital coordinate system is defined by three rotations.

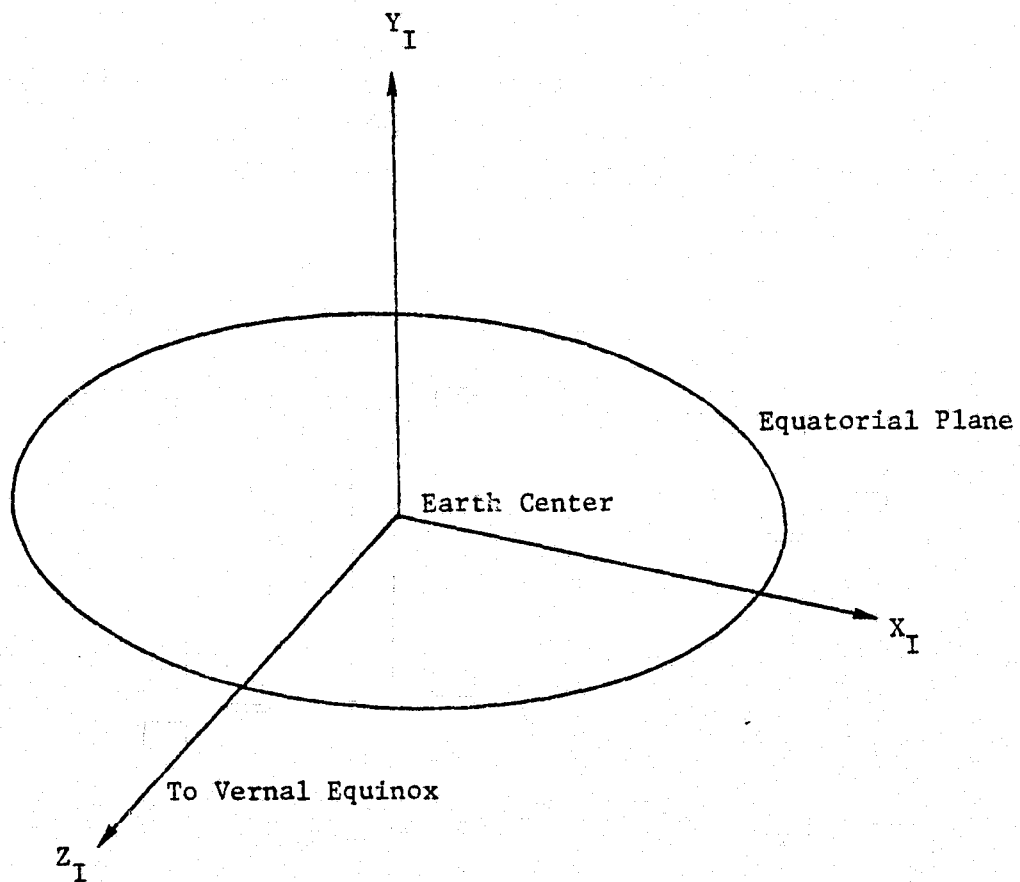


Figure 1. Geocentric Inertial Coordinate System.

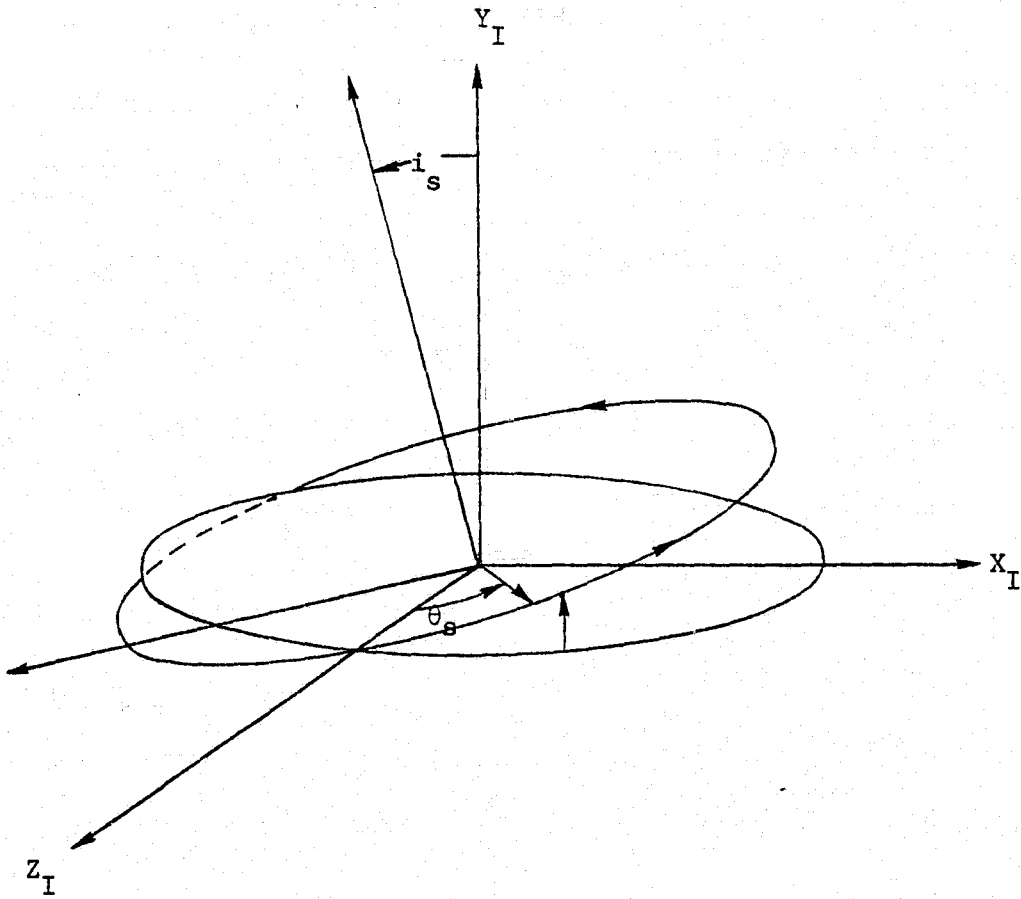


Figure 2. Geocentric Inertial and Sun Coordinate Systems.

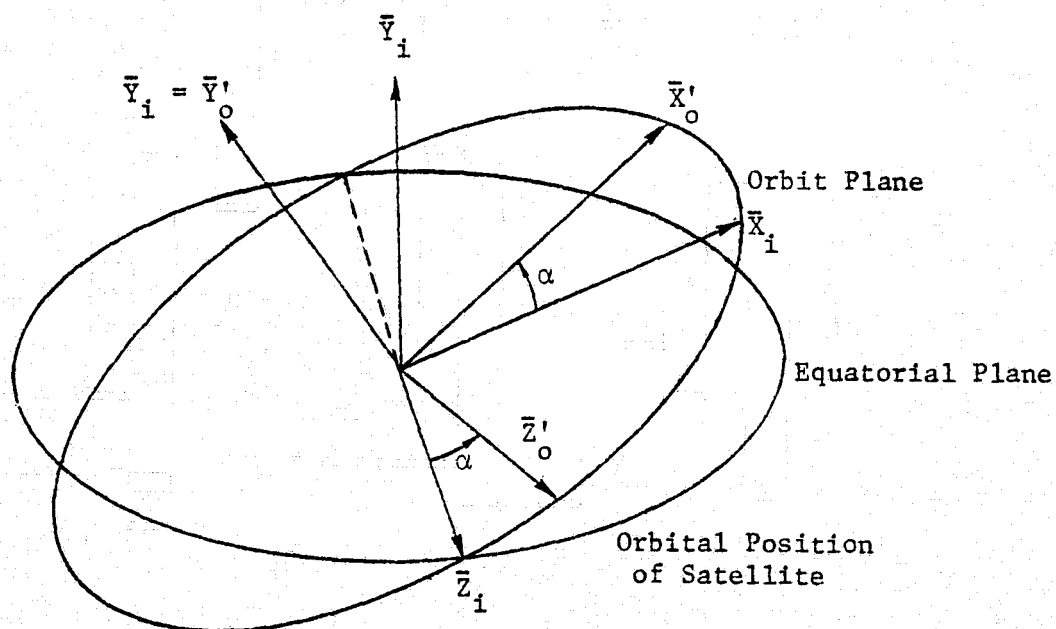
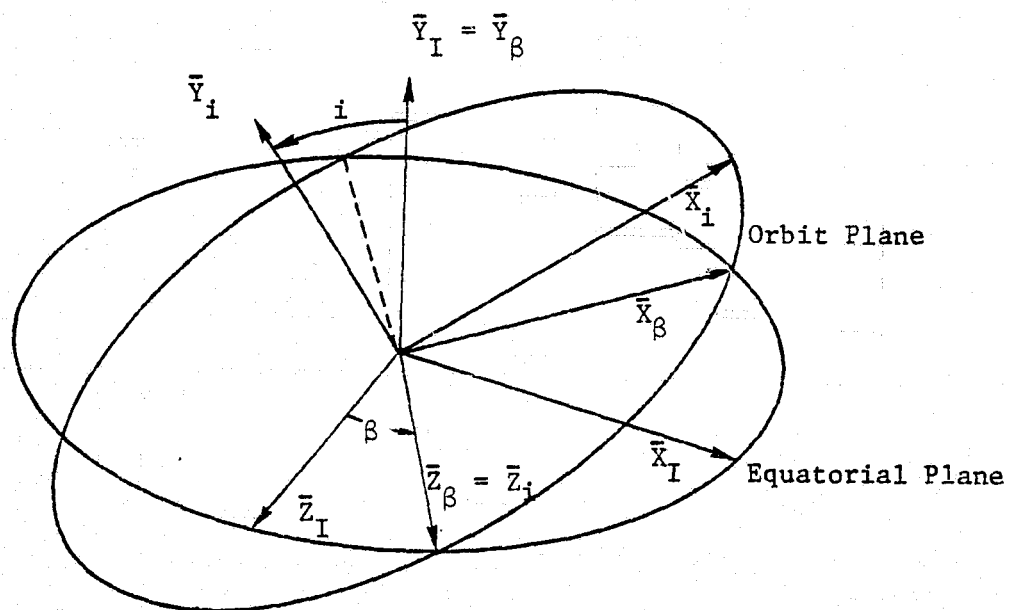


Figure 3. Inertial and Orbital Coordinate System.

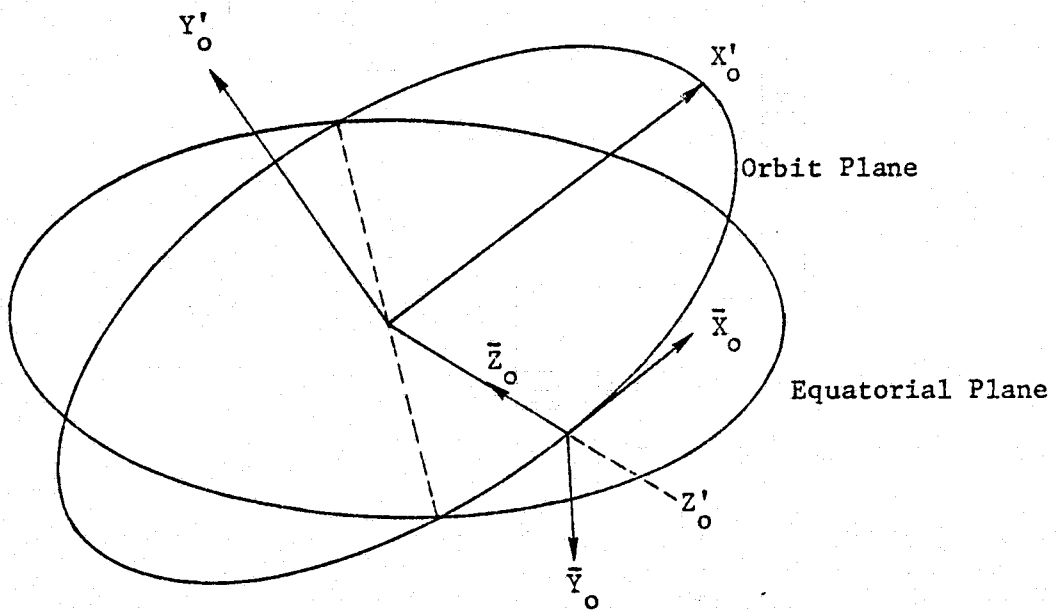
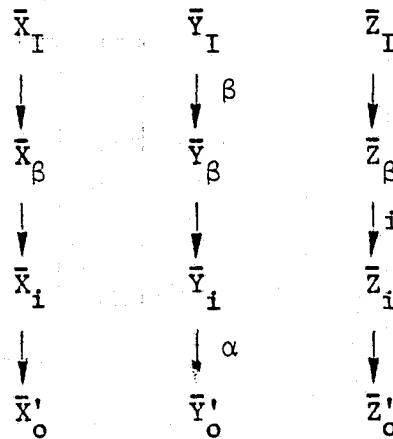


Figure 3. Inertial and Orbital Coordinate System (continued).



The three rotations are

A. Rotation about Y_I axis

$$\begin{bmatrix} \bar{X}_\beta \\ \bar{Y}_\beta \\ \bar{Z}_\beta \end{bmatrix} = \begin{bmatrix} \cos \beta & 0 & -\sin \beta \\ 0 & 1 & 0 \\ \sin \beta & 0 & \cos \beta \end{bmatrix} \begin{bmatrix} \bar{X}_I \\ \bar{Y}_I \\ \bar{Z}_I \end{bmatrix} \quad (4-A)$$

B. Rotation about Z_β axis

$$\begin{bmatrix} \bar{X}_i \\ \bar{Y}_i \\ \bar{Z}_i \end{bmatrix} = \begin{bmatrix} \cos i & \sin i & 0 \\ -\sin i & \cos i & 0 \\ 0 & 0 & 1 \end{bmatrix} \begin{bmatrix} \bar{X}_\beta \\ \bar{Y}_\beta \\ \bar{Z}_\beta \end{bmatrix} \quad (4-B)$$

C. Rotation about Y_i axis

$$\begin{bmatrix} \bar{X}'_0 \\ \bar{Y}'_0 \\ \bar{Z}'_0 \end{bmatrix} = \begin{bmatrix} \cos \alpha & 0 & -\sin \alpha \\ 0 & 1 & 0 \\ \sin \alpha & 0 & \cos \alpha \end{bmatrix} \begin{bmatrix} \bar{X}_i \\ \bar{Y}_i \\ \bar{Z}_i \end{bmatrix} \quad (4-C)$$

The orbital coordinate system will be denoted by:

$$[\bar{L}]_o = \begin{bmatrix} \bar{X}_o \\ \bar{Y}_o \\ \bar{Z}_o \end{bmatrix} \quad (5)$$

From Figure 3, the following transformation exists:

$$\begin{bmatrix} \bar{X}_o \\ \bar{Y}_o \\ \bar{Z}_o \end{bmatrix} = \begin{bmatrix} 1 & 0 & 0 \\ 0 & -1 & 0 \\ 0 & 0 & -1 \end{bmatrix} \begin{bmatrix} \bar{X}'_o \\ \bar{Y}'_o \\ \bar{Z}'_o \end{bmatrix} \quad (6)$$

From transformations (4) and (6) the transformation from inertial to the orbital coordinate system becomes

$$[L]_{o \rightarrow I} = \begin{bmatrix} (\cos \alpha \cos i \cos \beta - \sin \alpha \sin \beta) & (\cos \alpha \sin i) & (-\cos \alpha \cos i \sin \beta - \sin \alpha \cos \beta) \\ (\sin i \cos \beta) & (-\cos i) & (-\sin i \sin \beta) \\ (-\sin \alpha \cos i \cos \beta - \cos \alpha \sin \beta) & (-\sin \alpha \sin i) & (\sin \alpha \cos i \sin \beta - \cos \alpha \cos \beta) \end{bmatrix} \quad (7)$$

where

$$\begin{bmatrix} \bar{X}_o \\ \bar{Y}_o \\ \bar{Z}_o \end{bmatrix} = [L]_{o \rightarrow I} \begin{bmatrix} \bar{X}_I \\ \bar{Y}_I \\ \bar{Z}_I \end{bmatrix} \quad (8)$$

β is the right ascension of the orbit ascending node. The nodal regression rate is assumed constant, ⁽⁵⁾

$$\dot{\beta} = -0.001637 \left(\frac{R_e}{a}\right)^2 \frac{\pi}{1800P} \cos i \quad (9)$$

where P is the satellite orbital period in hours. i is the satellite orbit inclination with respect to the equatorial plane, and α is the satellite true anomaly; its initial displacement is measured from the ascending node for a circular orbit.

The body coordinate system is located at the center of mass of the satellite along its principal moments of inertia. The rotation from the orbital to the body coordinate system is illustrated in Figure 4. The order of transformation is defined as

$$\begin{array}{ccc}
 \bar{X}_0 & \bar{Y}_0 & \bar{Z}_0 \\
 \downarrow & \downarrow & \downarrow \psi \\
 \bar{X}_1 & \bar{Y}_1 & \bar{Z}_1 \\
 \downarrow & \downarrow \theta & \downarrow \\
 \bar{X}_2 & \bar{Y}_2 & \bar{Z}_2 \\
 \downarrow \phi & \downarrow & \downarrow \\
 \bar{X}_b & \bar{Y}_b & \bar{Z}_b
 \end{array} \tag{10}$$

The three Euler rotations are

A. Rotation about the \bar{Z}_0 axis

$$\begin{bmatrix} \bar{X}_1 \\ \bar{Y}_1 \\ \bar{Z}_1 \end{bmatrix} = \begin{bmatrix} \cos \psi & \sin \psi & 0 \\ -\sin \psi & \cos \psi & 0 \\ 0 & 0 & 1 \end{bmatrix} \begin{bmatrix} \bar{X}_0 \\ \bar{Y}_0 \\ \bar{Z}_0 \end{bmatrix} \tag{10-A}$$

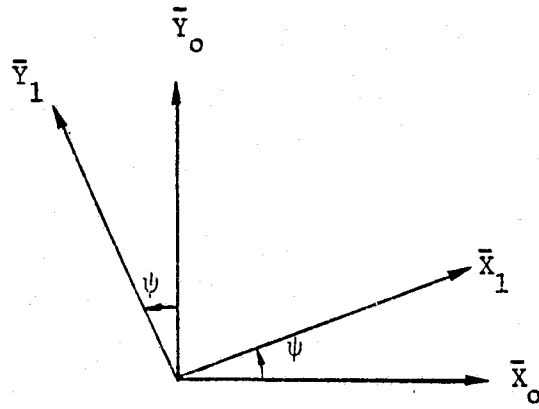
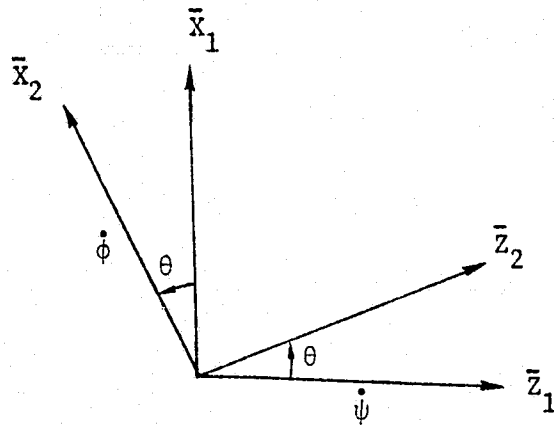
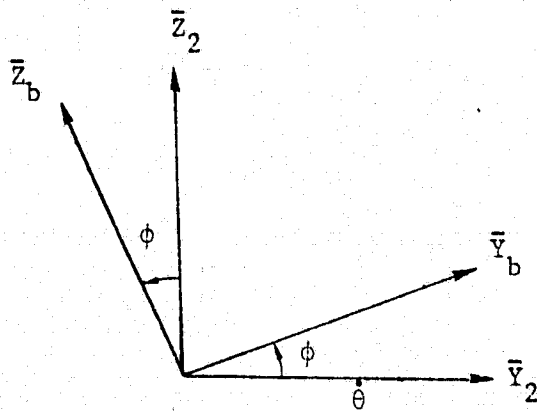
(a) Rotation of Angle ψ (b) Rotation of Angle θ (c) Rotation of Angle ϕ

Figure 4. Euler Rotations.

B. Rotation about the \bar{Y}_1 axis

$$\begin{bmatrix} \bar{X}_2 \\ \bar{Y}_2 \\ \bar{Z}_2 \end{bmatrix} = \begin{bmatrix} \cos \theta & 0 & -\sin \theta \\ 0 & 1 & 0 \\ \sin \theta & 0 & \cos \theta \end{bmatrix} \begin{bmatrix} \bar{X}_1 \\ \bar{Y}_1 \\ \bar{Z}_1 \end{bmatrix} \quad (10-B)$$

C. Rotation about the \bar{X}_2 axis

$$\begin{bmatrix} \bar{X}_b \\ \bar{Y}_b \\ \bar{Z}_b \end{bmatrix} = \begin{bmatrix} 1 & 0 & 0 \\ 0 & \cos \phi & \sin \phi \\ 0 & -\sin \phi & \cos \phi \end{bmatrix} \begin{bmatrix} \bar{X}_2 \\ \bar{Y}_2 \\ \bar{Z}_2 \end{bmatrix} \quad (10-C)$$

The transformation from orbital to the body coordinate system can be expressed as

$$[L]_{b \rightarrow o} = \begin{bmatrix} (\cos \theta \cos \psi) & (\cos \theta \sin \psi) & (-\sin \theta) \\ (\sin \phi \sin \theta \cos \psi - \cos \phi \sin \psi) & (\sin \phi \sin \theta \sin \psi + \cos \phi \cos \psi) & (\sin \phi \cos \theta) \\ (\cos \phi \sin \theta \cos \psi + \sin \phi \sin \psi) & (\cos \phi \sin \theta \sin \psi - \sin \phi \cos \psi) & (\cos \phi \cos \theta) \end{bmatrix} \quad (11)$$

where

$$\begin{bmatrix} \bar{X}_b \\ \bar{Y}_b \\ \bar{Z}_b \end{bmatrix} = [L]_{b \rightarrow o} \begin{bmatrix} \bar{X}_o \\ \bar{Y}_o \\ \bar{Z}_o \end{bmatrix} \quad (11-A)$$

The above transformations are basic in determining the attitude and position of the satellite. All rotations are defined positive by the right handed rotation rule. Any other transformations required are developed as needed.

CHAPTER III
DYNAMIC ANALYSIS

The motion of a satellite about its center of mass is described by Euler's moment equations which for the principal axes are⁽¹⁾

$$\begin{aligned} A \dot{\omega}_x + \omega_y \omega_z (C-B) &= M_x \\ B \dot{\omega}_y + \omega_x \omega_z (A-C) &= M_y \\ C \dot{\omega}_z + \omega_x \omega_y (B-A) &= M_z \end{aligned} \quad (12)$$

A, B, and C are the principal moments of inertia about the x, y, and z body axes, respectively. ω_x , ω_y , and ω_z are the satellite angular velocities. M_x , M_y , and M_z are the perturbing moments such as gravity-gradient torque.

Euler angular rates $\dot{\psi}$, $\dot{\theta}$, $\dot{\phi}$ describe the motion of the satellite with respect to a reference coordinate system which in this report is the orbital coordinate system. Euler angular rates can be expressed as a function of the body angular velocities and the Euler angles.

$$\begin{aligned} \dot{\phi} &= \omega_x + (\omega_y \sin\phi + \omega_z \cos\phi) \tan\theta \\ \dot{\theta} &= \omega_y \cos\phi - \omega_z \sin\phi \\ \dot{\psi} &= (\omega_y \sin\phi + \omega_z \cos\phi) \sec\theta \end{aligned} \quad (13)$$

The body angular velocities can also be written in terms of Euler rates.

$$\begin{aligned} \omega_x &= \dot{\phi} - \dot{\psi} \sin\theta \\ \omega_y &= \dot{\theta} \cos\phi + \dot{\psi} \cos\theta \sin\phi \\ \omega_z &= \dot{\psi} \cos\theta \cos\phi - \dot{\theta} \sin\phi \end{aligned} \quad (14)$$

Equation (12) can be expressed as

$$\begin{aligned}\dot{\omega}_x &= \frac{M_x(\phi, \theta, \psi)}{A} - \omega_y \omega_z \left(\frac{C-B}{A}\right) \\ \dot{\omega}_y &= \frac{M_y(\phi, \theta, \psi)}{B} - \omega_x \omega_z \left(\frac{A-C}{B}\right) \\ \dot{\omega}_z &= \frac{M_z(\phi, \theta, \psi)}{C} - \omega_x \omega_y \left(\frac{B-A}{C}\right)\end{aligned}\quad (15)$$

Knowing the perturbing moments as a function of the Euler angles equations (12) and (13) can be solved numerically. These equations describe the attitude motion and orientation of an asymmetric satellite.

The angular momentum, \bar{h} and energy, T of the satellite are computed from

$$\bar{h} = A\omega_x \bar{i}_b + B\omega_y \bar{j}_b + C\omega_z \bar{k}_b \quad (16)$$

$$T = \frac{1}{2} A\omega_x^2 + \frac{1}{2} B\omega_y^2 + \frac{1}{2} C\omega_z^2 \quad (17)$$

The position of the angular momentum vector in the orbital coordinate system with respect to the orbit radius vector and velocity vector tangent is shown in Figure 5. The angle δ is the angle between the radius vector of the earth and the satellite momentum vector.

$$\delta = \cos^{-1} \left(\frac{h_z}{h} \right)_o \quad 0^\circ \leq \delta \leq 180^\circ \quad (18-A)$$

h_z is the Z angular momentum component in the orbital coordinate system. The angle λ defines the angle between the angular momentum projection onto the x_o, y_o plane and the orbital velocity vector tangent.

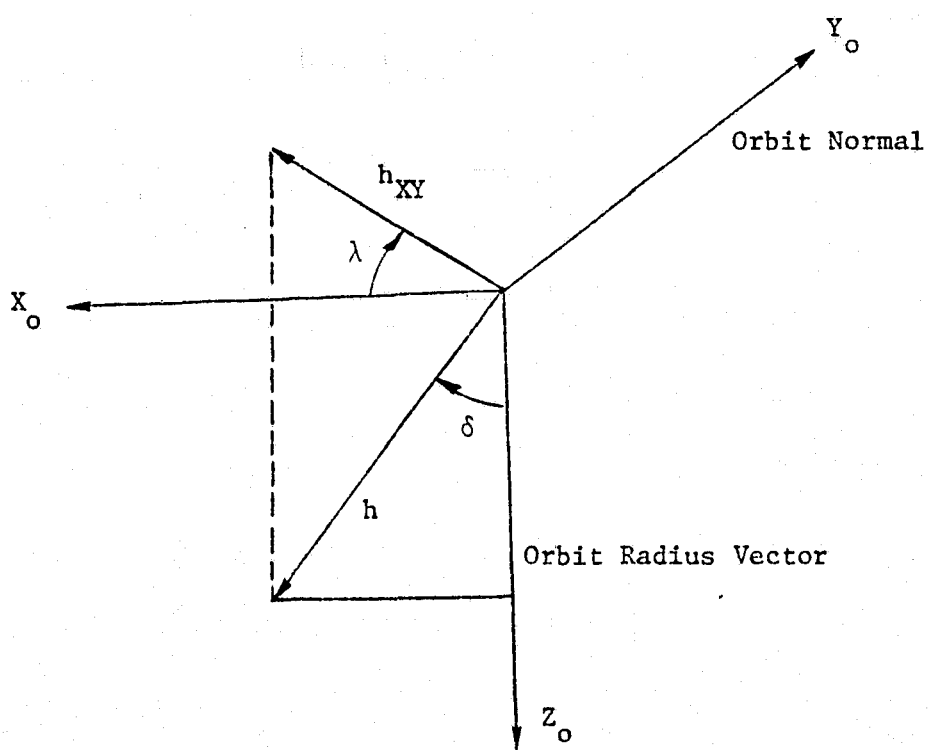


Figure 5. Nutation and Precession Angles in the Orbit Coordinate System.

$$\lambda = \tan^{-1} \left(\frac{h_x}{h_y} \right) \quad 0^\circ < \lambda \leq 360^\circ \quad (18-B)$$

h_x and h_y are the x and y angular momentum components in the orbital coordinate system, respectively. δ and λ will be noted as the nutation and precession angles in the orbital coordinate system.

The position of the minor axis with respect to the radius vector will be noted as the nadir angle, η . The nadir angle is defined as

$$\eta = \frac{\pi}{2} + \theta \quad (19)$$

CHAPTER IV
ENVIRONMENTAL PERTURBATION MODELS

Gravity-Gradient

Gravity-gradient torque is one of the major environmental perturbations for asymmetric satellites in near earth orbits.⁽⁶⁾ The gravity-gradient effect is a function of altitude, mass distribution, and the satellite orientation. Here the gravity torque model assumes a spherical earth neglecting anomalies due to its asymmetric mass distribution.

Under the assumption of a spherical earth, the gravity force field can be expressed as

$$d\bar{F}_G = \frac{-\mu dm}{r^3} \bar{r} \quad (20)$$

and the gravity-gradient torque as

$$(d\bar{M})_G = \bar{\rho} \times d\bar{F}_G \quad (21)$$

Figure 6 illustrates the coordinate system used in this derivation. $\bar{\rho}$ is the vector from the satellite center of mass to the mass element dm .

$$\bar{\rho} = x\bar{i}_b + y\bar{j}_b + z\bar{k}_b \quad (22)$$

Subscript b indicates the satellite body coordinate system. \bar{r} is the satellite radius vector from the geocenter to the mass element dm .

From Figure 6 the satellite radius vector \bar{R} can be written as

$$\bar{R} = -R \bar{k}_o \quad (23)$$

Transforming equation (23) to the satellite body coordinate system using equation (11), the radius vector can be expressed as

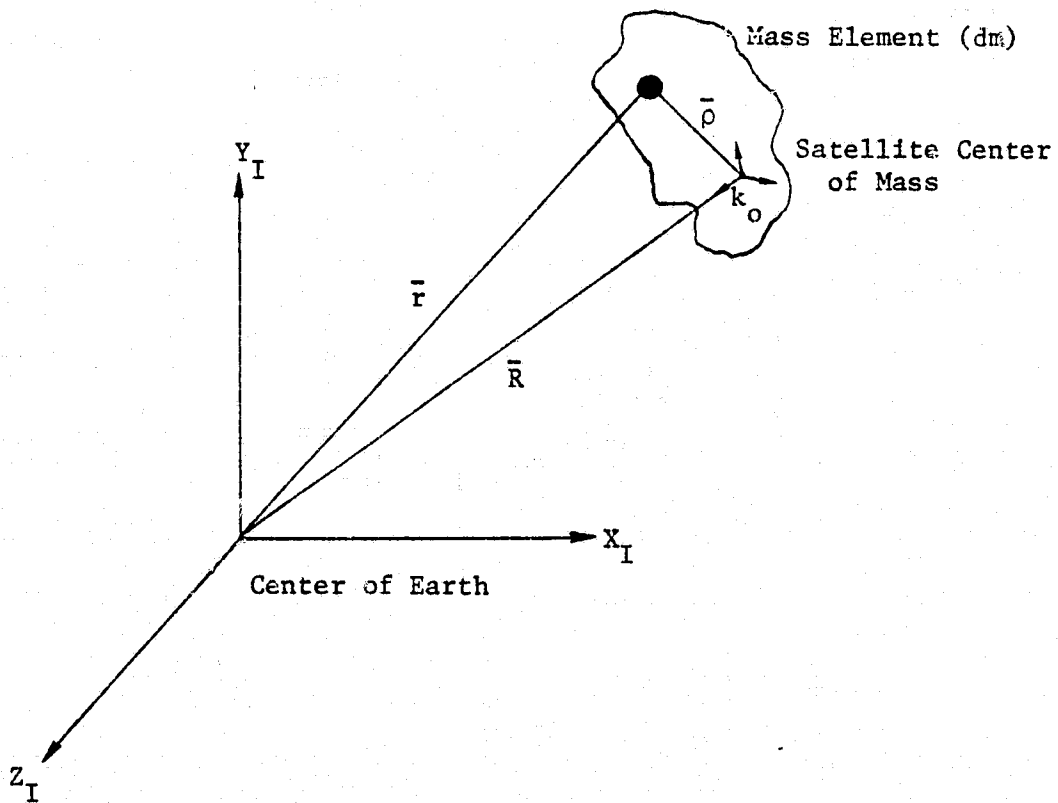


Figure 6. Coordinate System Used in Gravity-Gradient
Torque Derivations.

$$\bar{R}_b = R \sin\theta \bar{i}_b - R \sin\phi \cos\theta \bar{j}_b - R \cos\phi \cos\theta \bar{k}_b \quad (24)$$

Noting that $\bar{r} = \bar{R} + \bar{\rho}$ equation (21) becomes

$$(d\bar{M})_G = \bar{\rho} \times \left[-\frac{\mu}{r^3} (\bar{R} + \bar{\rho}) \right] \quad (25)$$

With the following approximations:

$$r^2 \approx R^2 \left[1 + \frac{2\bar{R} \cdot \bar{\rho}}{R^2} \right] \quad (26)$$

$$\frac{1}{r^3} \approx \frac{1}{R^3} \left[1 + \frac{2\bar{R} \cdot \bar{\rho}}{R^2} \right]^{-3/2} \quad (27)$$

$$\frac{1}{r^3} \approx \frac{1}{R^3} \left[1 - \frac{3\bar{R} \cdot \bar{\rho}}{R^2} \right] \quad (28)$$

$$\rho/R \ll 1 \quad (29)$$

Equation (25) becomes

$$d\bar{M}_G = \frac{-\mu}{R^3} \left[1 - \frac{3\bar{R} \cdot \bar{\rho}}{R^2} \right] [\bar{\rho} \times (\bar{R} + \bar{\rho})] dm \quad (30)$$

Since the coordinate system is located at the satellite center of mass the products of inertia are zero

$$\int \rho \, dm = 0 \quad (31)$$

$$I_{xy} = I_{xz} = I_{yz} = 0 \quad (32)$$

Integrating equation (30) results in the following equation for the gravity-gradient torque

$$\begin{aligned} \bar{M}_G = \frac{3\mu}{2R^3} [\sin 2\phi \cos^2 \theta (C-B) \bar{i}_b + \sin 2\theta \cos \phi (C-A) \bar{j}_b \\ + \sin 2\theta \sin \phi (A-B) \bar{k}_b] \end{aligned} \quad (33)$$

Equation (33) describes the gravity-gradient effect in satellite body coordinate system.

The gravity-gradient torque in the orbital coordinate system can be found by transforming equation (33) to the orbital coordinate system using the inverse of equation (11). The resulting torque equations in the orbital coordinate system are

$$\begin{aligned} (m_x)_o &= [(A-B) \sin 2\theta \sin \psi + (B-C) \{ \sin 2\theta \sin \psi \cos^2 \phi + \sin 2\phi \cos \theta \cos \psi \}] \frac{3\mu}{2R^3} \\ (m_y)_o &= [(B-A) \sin 2\theta \cos \psi + (C-B) \{ \cos^2 \phi \sin 2\theta \cos \psi - \sin 2\phi \cos \theta \sin \psi \}] \frac{3\mu}{2R^3} \\ (m_z)_o &= 0 \end{aligned} \quad (34)$$

$(m_x)_o$, $(m_y)_o$, and $(m_z)_o$ are the x, y, and z gravity-gradient components in the orbital coordinate system.

Aerodynamic Drag

Aerodynamic drag is a major perturbation for near earth satellites with altitudes of 800 km or less. Drag is a function of atmospheric density, angle of attack, satellite velocity and satellite shape. For complex satellite structures the satellite is divided into components of

spheres, flat plates, and cylinders. The center of pressure and moment arms for each component are computed. The total torque is computed from the sum of the components. For complex satellites shading of one component by another from the free stream flow may occur. This effect must be taken into account for an accurate drag model. Reference (7) describes a computer technique for modeling the shadow effect. The amount of one element shading another is a function of the orientation of the spacecraft with respect to the free stream velocity.

The aerodynamic torque can be expressed as

$$d\bar{M}_A = \sum_{i=1}^N \bar{\rho}_i \times dF_a \frac{\bar{V}_i}{V_i} \quad (35)$$

ρ_i is the distance from the center of mass to the center of pressure. \bar{V}_i is the relative velocity vector. dF_a is the aerodynamic force.

$$dF_a = \frac{1}{2} C_D \rho_a V^2 \cos \gamma_V dS_i \quad (36)$$

ρ_a is atmospheric density. C_D is the aerodynamic drag coefficient. V is the velocity at the surface element relative to incident stream. γ_V is the angle of attack of element dS . Equation (36) is the basic aerodynamic force equation. Reference (8) discusses aerodynamic force using normal and tangential momentum transfer coefficients to replace the drag coefficient.

For this report the aerodynamic drag model was developed by NASA⁽⁹⁾ for the Skylab vehicle. The drag model for Skylab was derived from data based on free molecular flow theory with a Knudsen number greater than 10. Three drag moment coefficients (c_x , c_y , c_z) as depicted in Figure 7

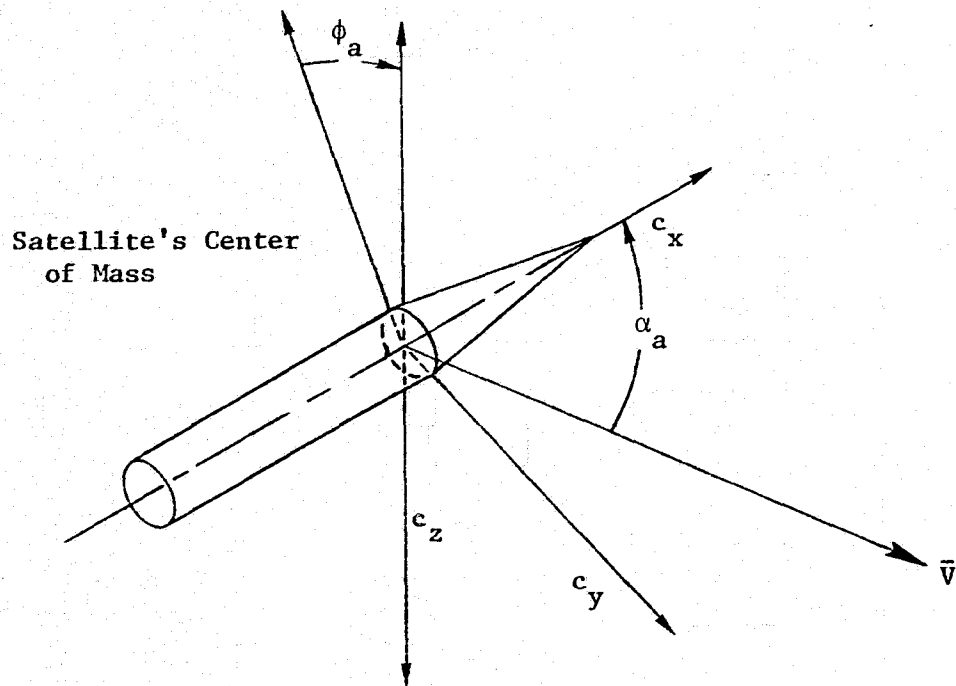


Figure 7. Aerodynamic Moment Coefficients in Satellite Body Coordinate System.

were computed for a number of orientations as a function of the angles (α_a, ϕ_a) . A Fourier series curve fit formula for c_x, c_y, c_z was derived from the above data as a function of the angles α_a and ϕ_a . $c_x, c_y,$ and c_z are the roll moment coefficient, pitching moment coefficient, and yaw moment coefficient, respectively. α_a and ϕ_a are the angle of attack and roll angle, respectively, as defined in Figure 7.

The resulting Fourier drag coefficient equations are

$$c(\alpha_a, \phi_a) = \frac{A_o(\phi_a)}{2} + \sum_{i=1}^m [A_i(\phi_a) \cos i\alpha_a + B_i(\phi_a) \sin i\alpha_a] \quad (37)$$

where

$$A_i(\phi_a) = \frac{a_{aio}}{2} + \sum_{j=1}^n [a_{aij} \cos j\phi_a + b_{aij} \sin j\phi_a] \quad (38-A)$$

(for $j = 2, 4, 6,$ and $i = 1, 3$)

$$B_i(\phi_a) = \frac{a_{bio}}{2} + \sum_{j=1}^n [a_{bij} \cos j\phi_a + b_{bij} \sin j\phi_a] \quad (38-B)$$

(for $j = 1, 3, 5,$ and $i = 1, 3$)

a_{ij} and b_{ij} are coefficients from Appendix B. The vehicle moment equations are computed from

$$\begin{aligned} M_x &= c_x q A_{ref} D_{ref} \\ M_y &= c_y q A_{ref} D_{ref} \\ M_z &= c_z q A_{ref} D_{ref} \end{aligned} \quad (39)$$

where

$$q = \frac{1}{2} \rho V^2$$

A_{ref} and D_{ref} are reference Area and Diameter of Skylab respectively, and are listed in Appendix C.

The roll angle ϕ_a and angle of attack α_a were computed from

$$\phi_a = \tan^{-1} \left[\frac{V_y}{V_z} \right]_b \quad 0 < \phi_a \leq 360^\circ \quad (40)$$

and

$$\alpha_a = \cos^{-1} \left[\frac{V_x}{V} \right]_b \quad 0 \leq \alpha_a \leq 180^\circ \quad (41)$$

as shown in Figure 7. Assuming a circular orbit for Skylab, where V_o is the orbital velocity,

$$\bar{V}_o = V_o \bar{i}_o$$

Expressing the velocity \bar{V}_o in body coordinates results in V_x , V_y , and V_z as required in equations (40) and (41)

$$\begin{aligned} \bar{V}_x &= V_o \cos\theta \cos\psi \bar{i}_b \\ \bar{V}_y &= V_o [\sin\phi \sin\theta \cos\psi - \cos\phi \sin\psi] \bar{j}_b \\ \bar{V}_z &= V_o [\cos\phi \sin\theta \cos\psi + \sin\phi \sin\psi] \bar{k}_b \end{aligned} \quad (42)$$

Appendix B lists the aerodynamic coefficients from Reference (9) used in computing the aerodynamic drag torques. The drag coefficients in Appendix B are based on Skylab with the auxiliary thermal shield, ATM solar arrays, and orbital workshop solar panel No. 1 deployed as shown in Figure 8.

The atmospheric density was calculated from the 1970 Jacchia atmosphere model described in reference (10). The following is a list of the effects causing atmospheric density variations used in the model:

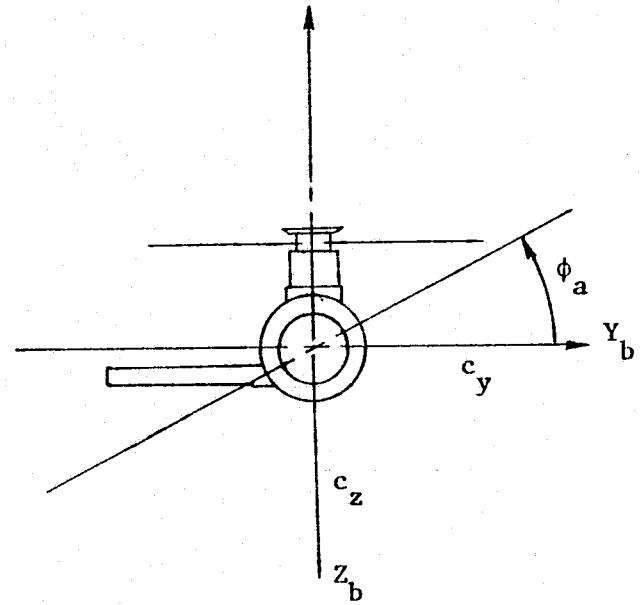
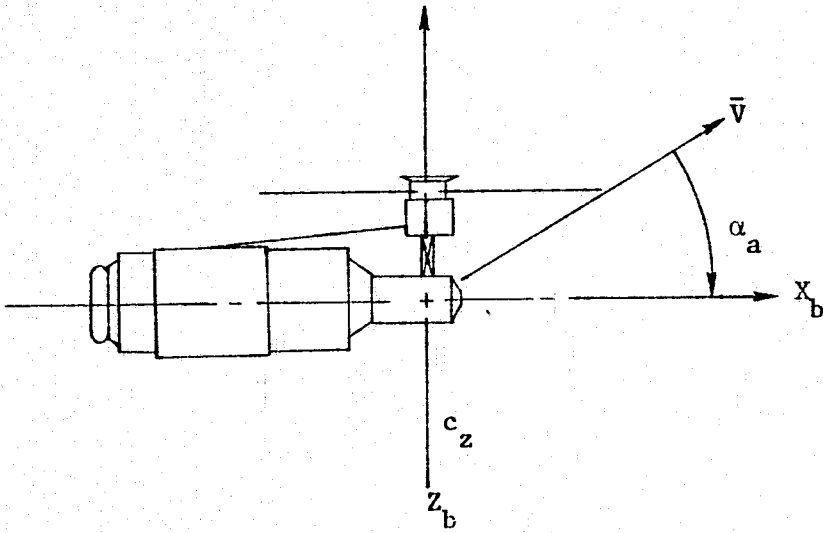
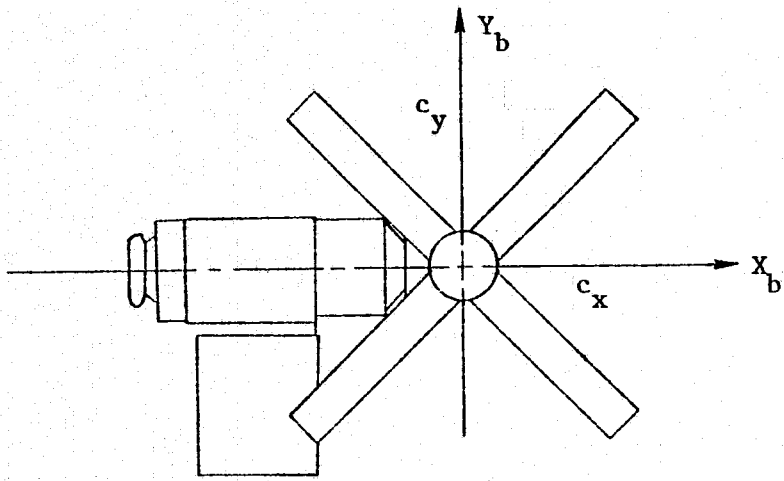


Figure 8. Skylab's Configuration for Aerodynamic Drag Model.

- (a) variations with an 11.5 year solar cycle
- (b) variations with daily changes in solar activity
- (c) diurnal variations
- (d) variations with geomagnetic activity
- (e) semiannual variations
- (f) seasonal-latitudinal variations of the lower thermosphere
- (g) seasonal-latitudinal variation of helium

The inputs are the sun and satellite right ascension and declination, number of days from January 1, 1970 and vehicle's altitude (km) above the surface of the earth. The output is the atmospheric density (kg/m^3) at the altitude of the satellite. The model calculates atmospheric densities for altitudes of 125 km to 700 km with a maximum error of 5% when compared to tabulated density values.

Magnetic Torque Model

Magnetic torques are caused by the interaction between the earth magnetic field and the satellite magnetic components. The earth magnetic field potential can be represented by a series of solid spherical harmonics. (11), (12) The magnetic field potential can be expressed as

$$V_m = R \sum_{N=1}^{N=8} \sum_{K=0}^{K=N} \left(\frac{R}{R_e}\right)^{N+1} [g_N^K \cos K\lambda_M + h_N^K \sin K\lambda_M] p_N^K (\cos \theta_M) \quad (43)$$

The spherical magnetic force components are

$$\bar{e}_\theta = \sum_{N=1}^{N=8} \sum_{K=0}^{K=N} \left(\frac{R}{R_e}\right)^{N+2} [g_N^K \cos K\lambda_M + h_N^K \sin K\lambda_M] \frac{d}{d\theta} p_N^K (\cos \theta_M) \quad (44)$$

$$\bar{e}_\lambda = \sum_{N=1}^{N=8} \sum_{K=0}^{K=N} \left(\frac{R}{R_e}\right)^{N+2} \frac{-K}{\sin\theta} [-g_N^K \sin K\lambda_M + h_N^K \cos K\lambda_M] p_N^K(\cos\theta_M) \quad (45)$$

$$\bar{e}_r = \sum_{N=1}^{N=8} \sum_{K=0}^{K=N} -(N+1) \left(\frac{R}{R_e}\right)^{N+2} [g_N^K \cos K\lambda_M + h_N^K \sin K\lambda_M] p_N^K(\cos\theta_M) \quad (46)$$

where:

\bar{e}_θ , \bar{e}_λ , and \bar{e}_r are the magnetic spherical force components in a geocentric coordinate reference with respect to the Greenwich time line as shown in Figure 9. λ_M is the east longitude from the Greenwich line and θ_M is the colatitude. R is the satellite orbit radius and R_e the earth radius.

The function $p_N^K(\cos(\theta_M))$ is defined as

$$p_N^K(v) = \frac{1}{2^N N!} \left[\frac{\epsilon_K (N-K)! (1-v^2)^K}{(N+K)!} \right]^{1/2} \frac{d^{(K+N)} (v^2-1)^N}{dv^{(K+N)}} \quad (47)$$

where

$$\begin{aligned} v &= \cos \theta_M \\ \epsilon_K &= 1 \text{ for } K = 0 \\ \epsilon_K &= 2 \text{ for } K \geq 1 \end{aligned} \quad (48)$$

The epoch time for this model is 1965.⁽¹¹⁾ Since the magnetic field varies with time, the coefficients g_N^K and h_N^K are functions of time

$$C_N^K(t) = C_N^K(t_0) + \dot{C}_N^K \quad (49)$$

Reference 12 lists the magnetic coefficients g_N^K and h_N^K at epoch 1965 with associated secular coefficients \dot{g}_N^K and \dot{h}_N^K .

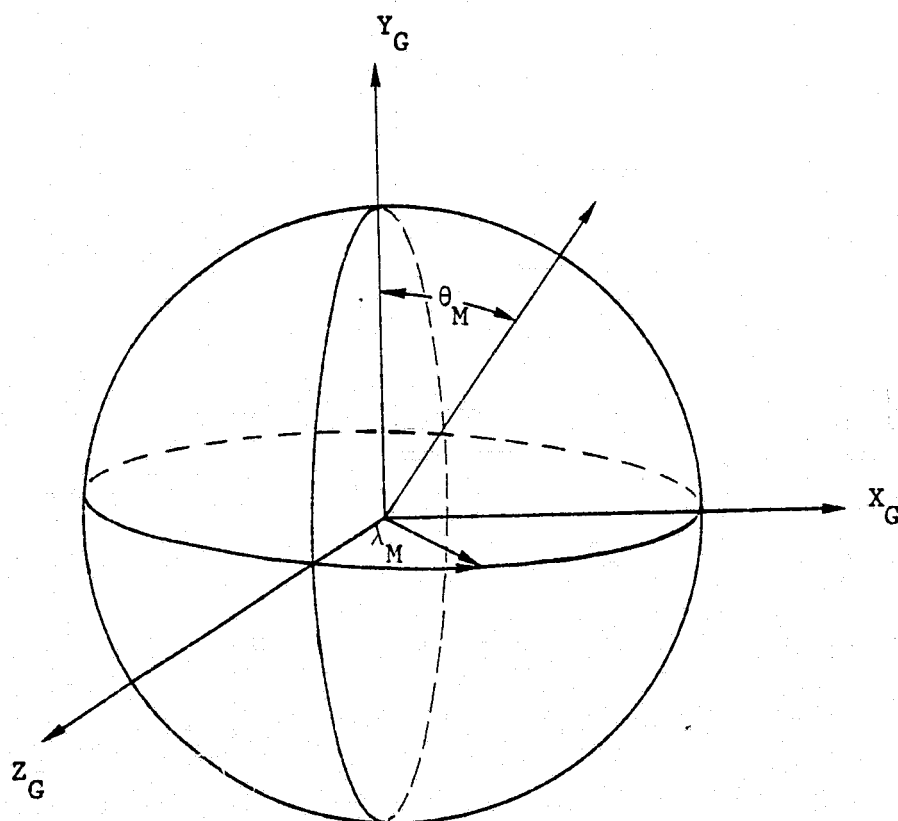


Figure 9. Coordinate System for the Earth's
Magnetic Field Model.

The earth's magnetic field components can be transformed to a geocentric Greenwich coordinate system with Z_G passing through the Greenwich line as shown in Figure 9 by

$$\begin{bmatrix} \bar{e}_x \\ \bar{e}_y \\ \bar{e}_z \end{bmatrix}_G = [L]_{G \rightarrow S} \begin{bmatrix} \bar{e}_\lambda \\ \bar{e}_\theta \\ \bar{e}_r \end{bmatrix} \quad (50)$$

where

$$[L]_{G \rightarrow S} = \begin{bmatrix} \cos \lambda_M & -\cos \theta_M \sin \lambda_M & \sin \theta_M \sin \lambda_M \\ 0 & \sin \theta_M & \cos \theta_M \\ -\sin \lambda_M & -\cos \theta_M \cos \lambda_M & \sin \theta_M \cos \lambda_M \end{bmatrix} \quad (51)$$

The Greenwich geocentric coordinate system is related to the geocentric inertial coordinate system by

$$\begin{bmatrix} \bar{X} \\ \bar{Y} \\ \bar{Z} \end{bmatrix}_I = [L]_{I \rightarrow G} \begin{bmatrix} \bar{e}_x \\ \bar{e}_y \\ \bar{e}_z \end{bmatrix}_G \quad (52)$$

where

$$[L]_{I \rightarrow G} = \begin{bmatrix} \cos \lambda_0 & 0 & -\sin \lambda_0 \\ 0 & 1 & 0 \\ \sin \lambda_0 & 0 & \cos \lambda_0 \end{bmatrix} \quad (53)$$

λ_0 is defined as $\lambda_i + \Omega_e t$. λ_i is the initial angle of the Greenwich line from the vernal equinox. Ω_e is the earth rotation rate.

The magnetic torque is computed from

$$\bar{M}_m = \bar{M} \times \bar{B} \quad (54)$$

where \bar{M} and \bar{B} are the satellite magnetic moment and the earth magnetic field vector, respectively.

Solar Radiation Pressure

Solar radiation torques are due to the incoming solar radiation flux of the sun. The solar torques are functions of the distance from the sun, satellite surface geometry, and surface reflectivity. Only direct radiation from the sun is considered. Earth and atmospheric reflected radiation along with the satellite radiation are ignored. In this paper the secular and periodic terms are separated by averaging one orbit, assuming a constant inertial solar radiation force.

The physical model used is similar to the model in reference (13). Figure 10 shows the geometry of the model. The solar radiation force is due to the reflected and absorbed components of the incoming sun radiation flux

$$d\bar{F}_s = d\bar{F}_i + d\bar{F}_r \quad (55-A)$$

where F_i and F_r are the absorbed and reflected solar radiation forces, respectively. Assuming secular reflection, angles γ_1 and γ_2 are equal.

$$\gamma_1 = \gamma_2 = \gamma \quad (55-B)$$

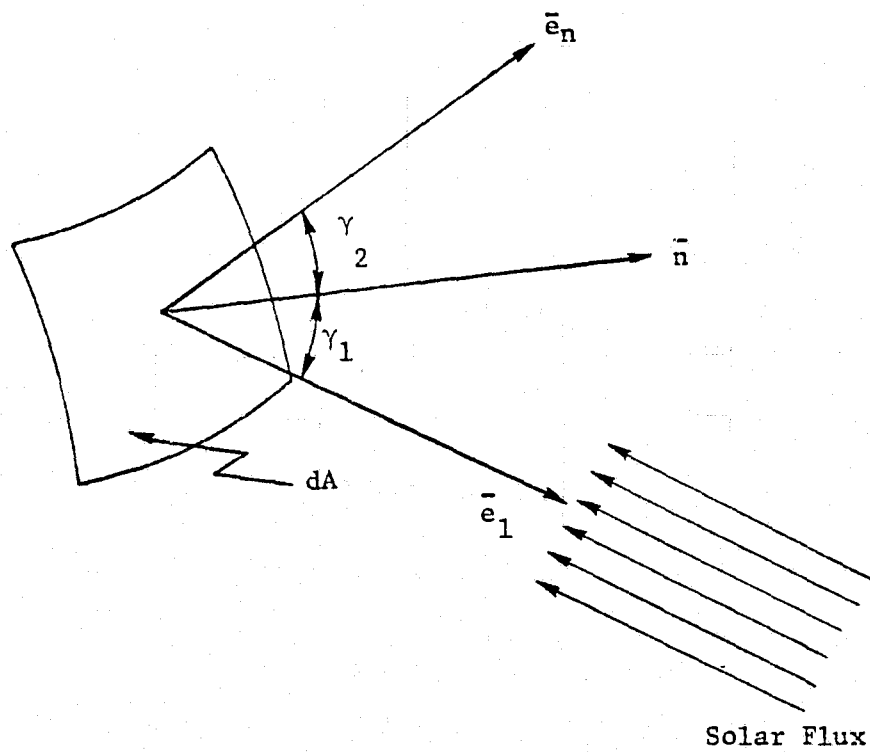


Figure 10. Geometry for the Solar Radiation
Physical Model.

From Figure 10, \bar{e}_1 is in the opposite direction of the incoming radiation flux vector. \bar{n} is defined as the unit vector normal to the surface element dA . The incident force component can be written as

$$d\bar{F}_i = - (S_r + S_A) P_S dA \bar{e}_1 \quad (56)$$

where

S_A = satellite surface absorption coefficient

S_r = satellite surface reflection coefficient

P_S = solar radiation pressure

dA = element area

The reflected force component is

$$d\bar{F}_r = - S_r P_S dA \bar{e}_2 \quad (57)$$

where \bar{e}_2 is defined in Figure 10. From equations 56 and 57 the total solar radiation force is

$$d\bar{F}_s = - P_S dA [(S_r + S_A) \bar{e}_1 + S_r \bar{e}_2] \quad (58)$$

The total solar radiation force can be expressed in terms of the incoming flux vector (\bar{e}_1) and the surface normal vector (\bar{n}).

$$d\bar{F}_s = - P_S dA [(S_A + 2S_r) \cos\gamma \bar{n} + S_A \bar{n} + (\bar{e}_1 \times \bar{n})] \quad (59)$$

The solar force components expressed in geocentric inertial components are

$$\begin{aligned} \bar{F}_x &= -F_s \sin \theta_s \cos i_s \\ \bar{F}_y &= -F_s \sin \theta_s \sin i_s \\ \bar{F}_z &= -F_s \cos \theta_s \end{aligned} \quad (60)$$

Since the initial secular trends were of interest, the periodic and secular terms were separated whenever possible. For the solar radiation force the inertial force components were assumed constant over one orbit. The inertial components were transformed to the orbital reference coordinate system and averaged over an orbit as a function of true anomaly.

$$\bar{\mathbf{F}}_{\text{avg}} = \frac{1}{2\pi} \int_0^{2\pi} \bar{\mathbf{F}}_s \, d\alpha \quad (61)$$

$$\begin{bmatrix} F_x \\ F_y \\ F_z \end{bmatrix}_O = L_{O \rightarrow I} \begin{bmatrix} F_x \\ F_y \\ F_z \end{bmatrix}_I \quad (62)$$

becomes

$$\begin{bmatrix} F_x \\ F_y \\ F_z \end{bmatrix}_O = [L_{O \rightarrow I}]_{\text{avg}} \begin{bmatrix} F_x \\ F_y \\ F_z \end{bmatrix}_I \quad (63)$$

where

$$[L_{O \rightarrow I}]_{\text{avg}} = \begin{bmatrix} (\cos\alpha \cos i \cos\beta - \sin\alpha \sin\beta) & 0 \\ \sin i \cos\beta & -\cos i \\ (-\sin\alpha \cos i \cos\beta - \cos\alpha \sin\beta) & 0 \\ (-\cos\alpha \cos i \sin\beta - \sin\alpha \cos\beta) \\ -\sin i \sin\beta \\ (\sin\alpha \cos i \sin\beta - \cos\alpha \cos\beta) \end{bmatrix} \quad (64)$$

Equation (64) assumes i , F_x , F_y , and F_z are constant over one orbit. The ascending node was not assumed constant. As the orbit inclination approaches 90 degrees, $\dot{\beta}$ approaches zero. Therefore, if β is assumed constant the transformation, equation (64), after averaging becomes

$$[L_{O \rightarrow I}]_{\text{avg}} = \begin{bmatrix} 0 & 0 & 0 \\ \sin i \cos \beta & -\cos i & -\sin i \sin \beta \\ 0 & 0 & 0 \end{bmatrix} \quad (65)$$

To predict accurately long term effects the apparent motion of the sun needs to be included. In this study we were concerned with initial secular effects in determining the trends of the satellite attitude motion. The apparent motion of the sun was assumed constant.

After averaging the solar forces, the orbital force components were transformed to the body reference coordinates. The final averaged force components, therefore, can be expressed in matrix notation as

$$\begin{bmatrix} \bar{F}_x \\ \bar{F}_y \\ \bar{F}_z \end{bmatrix}_b = [L_{b \rightarrow O}] [L_{O \rightarrow I}]_{\text{avg}} \begin{bmatrix} \bar{F}_x \\ \bar{F}_y \\ \bar{F}_z \end{bmatrix}_I \quad (66)$$

The solar torques are computed from the cross-product

$$d\bar{M}_S = \sum_{i=1}^N (\bar{\rho}_i \times d\bar{F}_S) \quad (67)$$

where ρ_i is the distance between the center of mass and center of pressure of the satellite. N is the number of satellite components.

The shadow model is used to determine the points at which the satellite enters and leaves the earth shadow by assuming the projection

of the shadow to be a cylinder. The model is shown in Figure 11 and assumes the earth, sun, and satellite to be coplanar.

\bar{L}_S is the unit vector from the earth to the sun.

$$\bar{L}_S = \sin\theta_s \cos i_s \bar{i}_I + \sin\theta_s \sin i_s \bar{j}_I + \cos\theta_s \bar{k}_I \quad (68)$$

From Figure 11 the angle D can be defined as

$$\cos D = \frac{\bar{L}_S \cdot \bar{r}}{r} \quad (69)$$

For $\cos D > 0$, the satellite is in sunlight; for $\cos D < 0$ the satellite is in the shadow of the earth. Also from Figure 11 angle E can be written as

$$\sin E = R_e / r \quad (70)$$

Considering Figure (11) geometry the following condition exists;

if $(D + E) < 180^\circ$; satellite is in sunlight

if $(D + E) > 180^\circ$; satellite is in earth's shadow

The identity

$$\sin (D + E) = \sin D \cos E + \sin E \cos D \quad (71)$$

was used in the computer program for this test.

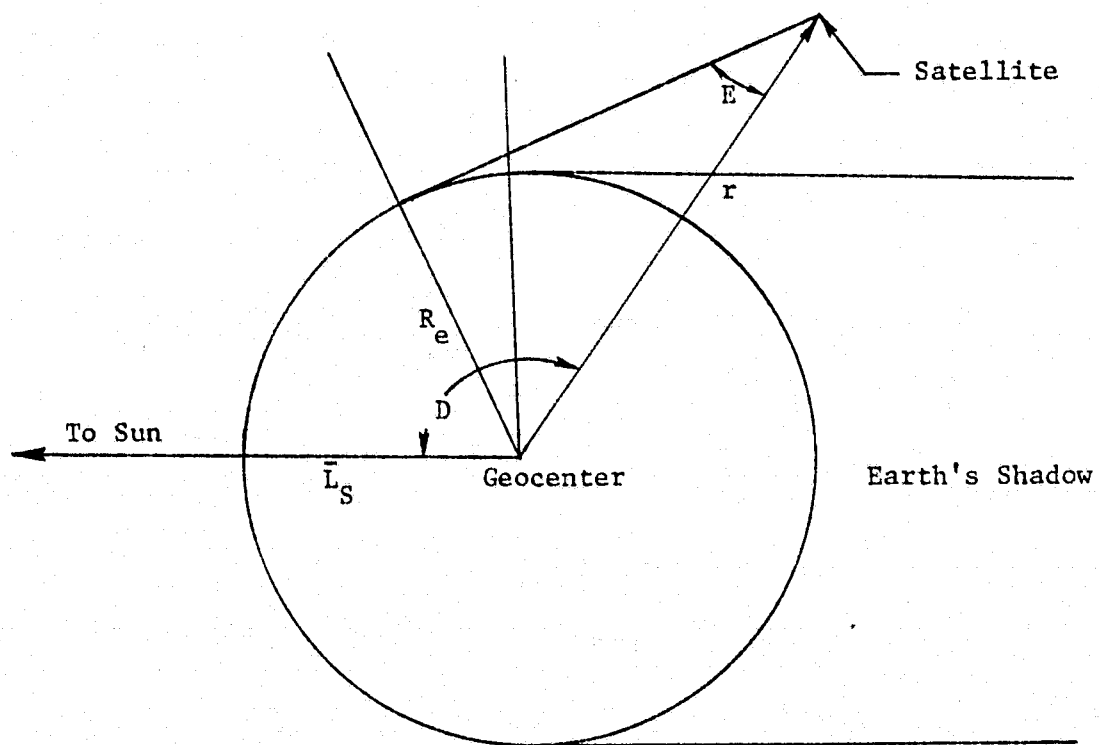


Figure 11. Geometry for the Shadow Model.

CHAPTER V
APPLICATION TO SKYLAB

The Euler moment equations discussed in Chapter III were solved numerically using an IBM 370/168 computer for the Skylab spacecraft. The equations were solved using a fourth-order Runge-Kutta method and a fourth-order modified Adams-Bashforth predictor corrector method with a constant integration step size.⁽¹⁴⁾ The fourth order Runge-Kutta method was used to compute the starting values for the Adams-Bashforth predictor-corrector. After the starting values were computed the predictor-corrector algorithm was used to integrate the equations of motion.

The Euler's moment equations were solved for the slow tumbling Skylab spacecraft using initial conditions in Appendix A. The slow tumble case simulates a slow spin approximately about the major axis. The slow tumble was solved for the torque-free motion, gravity-gradient, aerodynamic drag, solar radiation pressure, and gravity-gradient with aerodynamic torque. Results from each perturbation are discussed in Chapter VI.

Since the solution of Euler's attitude equations used excessive computer time only the initial effect of the perturbations on the spacecraft were simulated. The torque-free motion is discussed first, followed by the environmental effects.

The magnetic effects were not studied since data was not available on the magnetic residual moments of Skylab; they were assumed to be negligible. Solar radiation effects were simulated and found to be negligible compared to aerodynamic drag and gravity-gradient torques.

CHAPTER VI

SIMULATION RESULTS

Torque-Free Results

Since the general torque-free solution to Euler's attitude equations are elliptic functions, equation (12) was solved numerically to determine the force-free motion in the orbital and satellite coordinate system for Skylab, using the initial conditions in Appendix A. The motion in the orbital coordinate system of the satellite angular momentum vector is represented in Figure 12 for approximately five orbits. The nutation and precession angles are defined by equation (18). The rapid motion at 40, 90, and 140 minutes is caused by the singularity of the Euler Angle θ . As θ approaches 90 degrees the Euler rates $(\dot{\phi}, \dot{\psi})$ become larger as shown by equation (13). This causes the angular momentum to be transferred from either x or y to the y or x axis inducing a large angular momentum precession rate for a short duration. At $t = 180$ minutes the precession angle changes direction and the angular momentum vector passes above the orbit plane (nutation angle $> 90^\circ$). The nutation angle varies from 70 to 116 degrees and the precession angle varies from 40 to 326 degrees. Figure 12 illustrates the motion of the angular momentum vector in the orbital coordinate system.

The nadir angle (λ) represents the angular motion of the minor (x) axis with respect to the orbit radius vector. Figure 13 illustrates the nadir angle for the slow tumble torque free solution. From Figure 13 the nadir angle oscillates between 0 and 180 degrees. The nadir angle

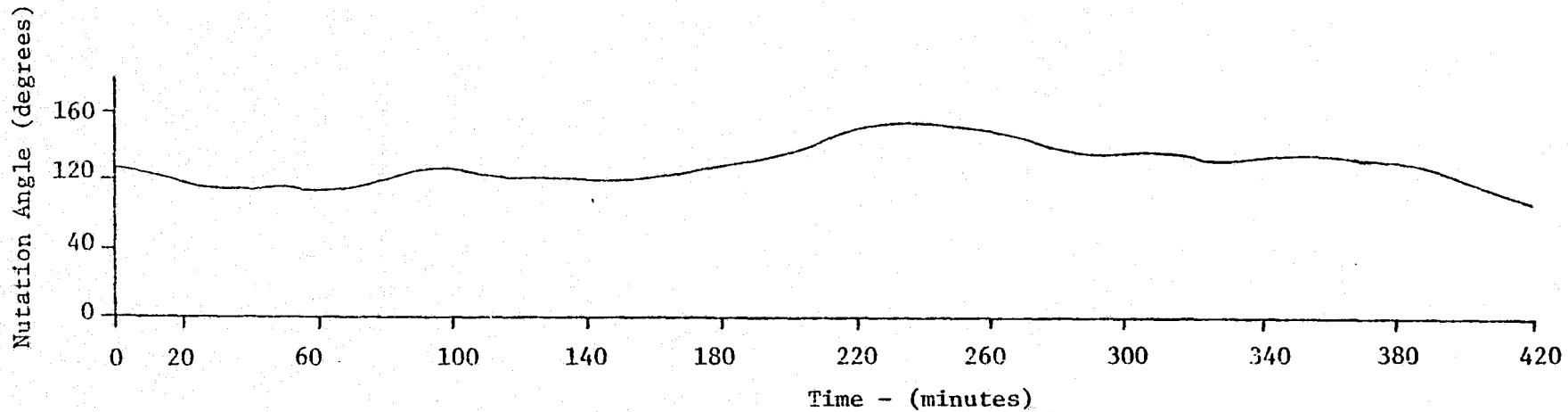
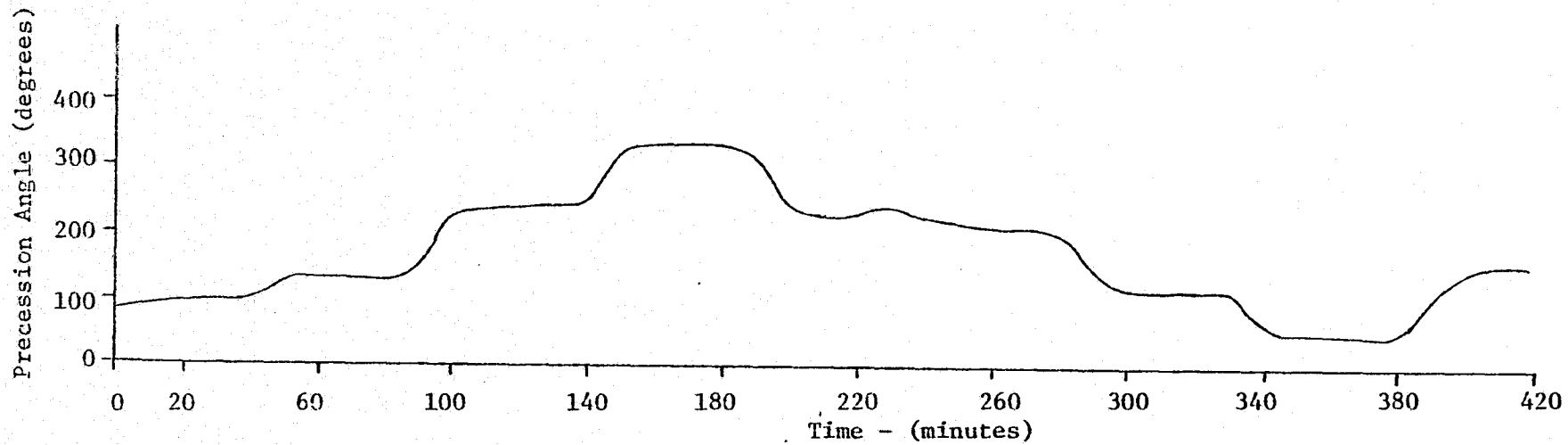


Figure 12. Nutation and Precession Angles for the Torque-Free Solution.

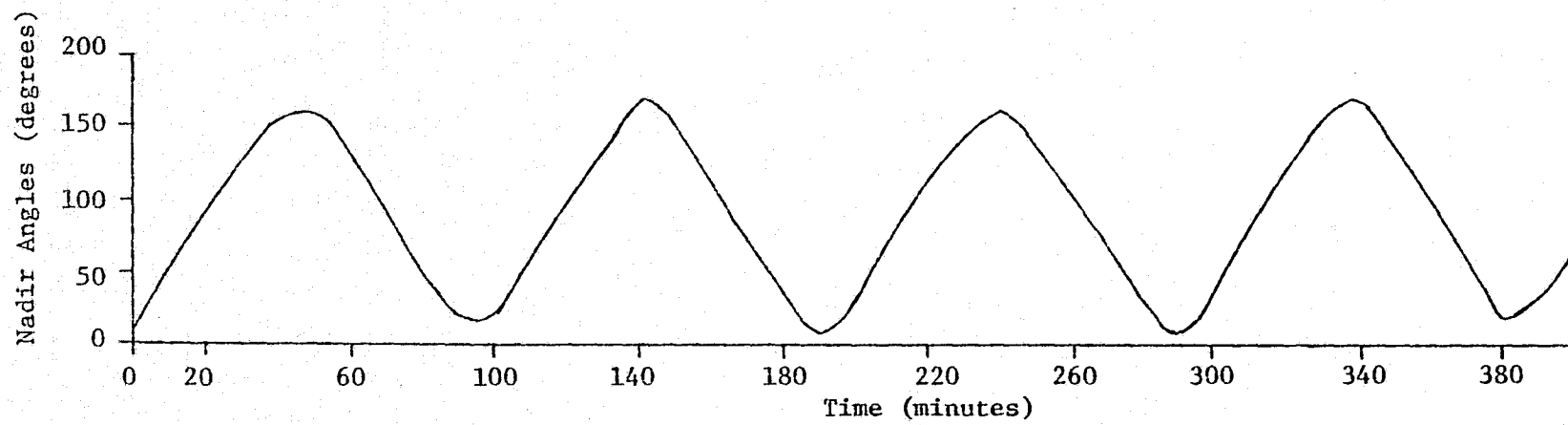


Figure 13. Nadir Angle for Torque-Free Solution.

period is approximately two orbits. The angular momentum and energy for the slow tumble case were $4227 \text{ kg}\cdot\text{m}^2/\text{s}$ and $2.37 \text{ kg}\cdot\text{m}^2/\text{s}^2$.

Gravity-Gradient Results

The result of the gravity-gradient torque on the nadir angle is illustrated in Figure 14 which shows that the nadir angle is bound between 0 and 40 degrees. Comparing Figures 13 and 14 the gravity-gradient torque tends to align the minor axis along the orbit radius vector. From inspection of equation (33) an equilibrium position (zero torque) state exists when the minor axis is aligned along the orbit radius vector. This state occurs when the nadir angle is 0 or 180 degrees ($\theta = \pm 90^\circ$). Another equilibrium position exists when all principal axes are aligned along the orbital coordinate system axes. As shown by equation (33) any misalignment of the principal axes from the orbital coordinate system induces a torque. Once a misalignment occurs gravity-gradient torques will attempt to orient the satellite toward an equilibrium state. Comparing the torque-free solution in Figure 13 and the gravity-gradient solution in Figure 14, the amplitude of the nadir angle oscillation is reduced from 180 degrees for the torque-free case to 40 degrees for the gravity-gradient case. The nadir angle period of oscillation decreases from 184 minutes to 66 minutes. Thus, by bounding the amplitude of the nadir angle oscillations gravity-gradient torque causes the frequency of the oscillations to increase.

Figure 15 illustrates the gravity-gradient effect on Skylab's energy and angular momentum. Gravity-gradients cause the energy and angular momentum to become cyclic with a period of 34.1 minutes or approximately .36 of an orbital period. From the initial conditions the

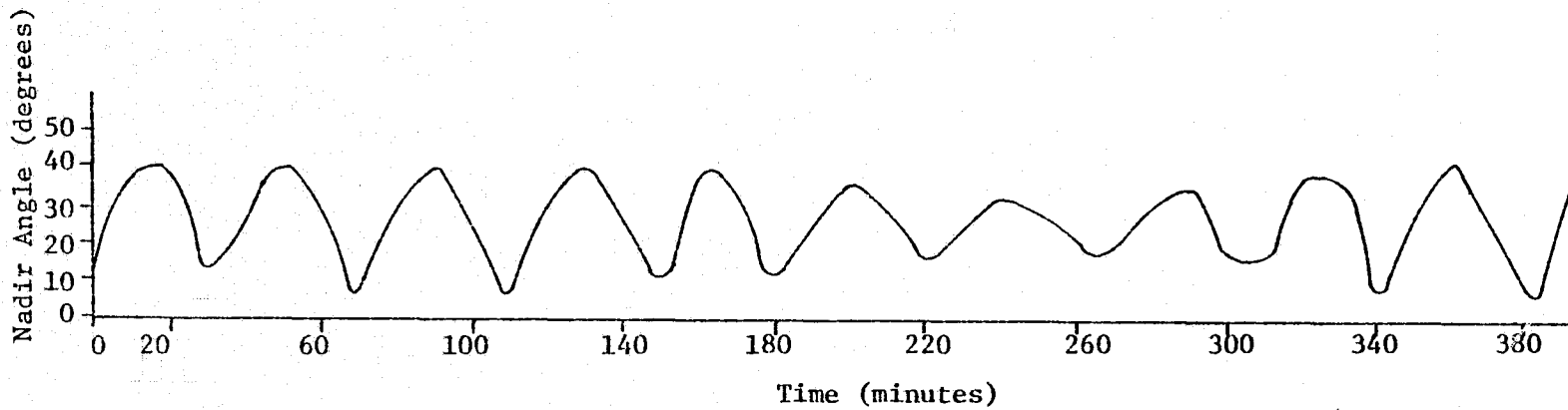


Figure 14. Nadir Angle for Gravity-Gradient.

REPRODUCIBILITY OF THIS
ORIGINAL PAGE IS POOR

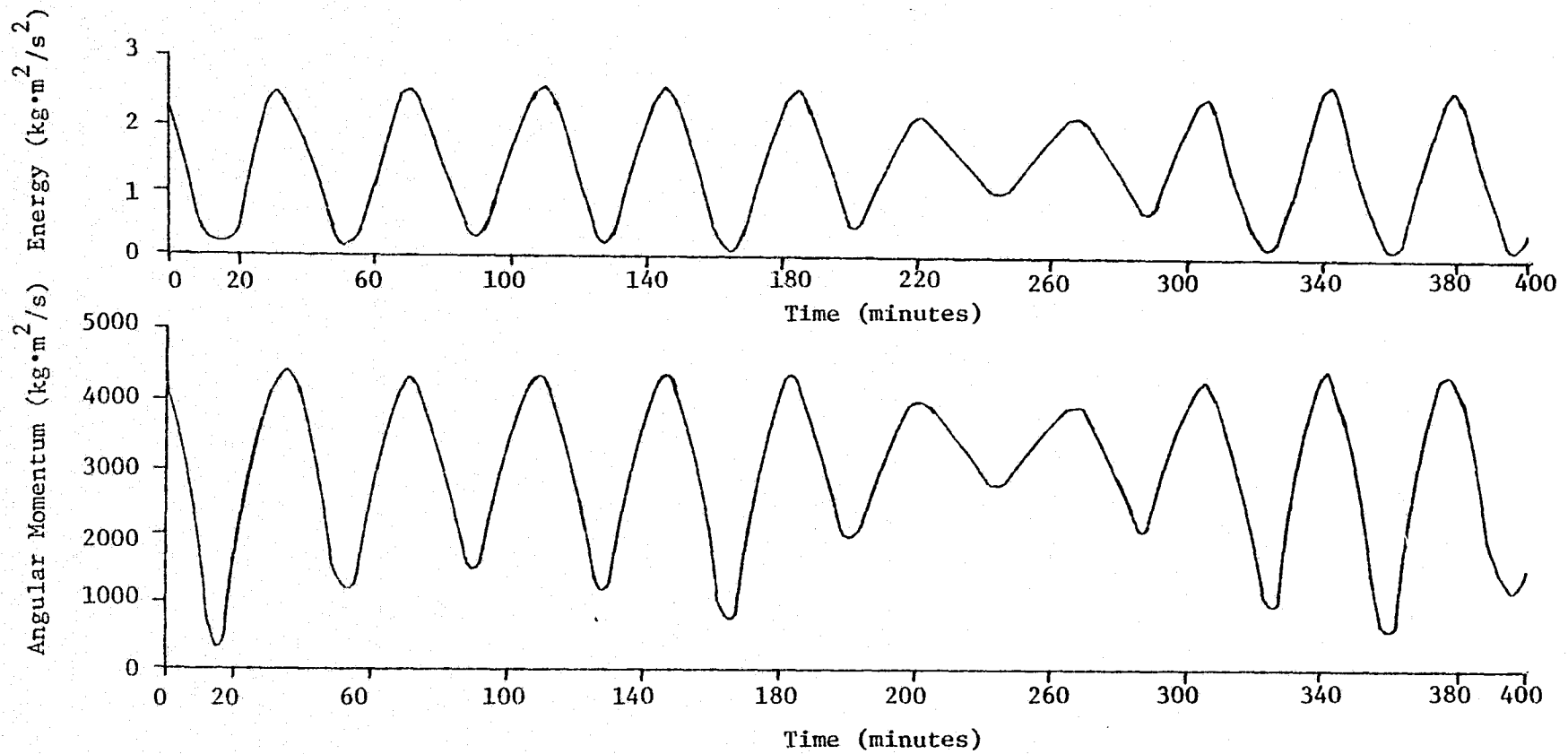


Figure 15. Effect of Gravity-Gradient on the Angular Momentum and Energy.

spacecraft was near a zero-torque ($\theta = -80^\circ$) position initially. As the spacecraft moves from the initial position gravity-gradient torques attempt to restore it, decreasing the angular momentum and energy. As a result angular momentum and energy are maximum when the satellite nadir angle is minimum and vice versa. Figures 14 and 15 illustrate this effect.

The motion of the angular momentum vector in the orbital coordinate system is shown in Figure 16. The gravity-gradient torque causes the precession angle and rate to become periodic with an approximate period of fifty minutes. The singularity due to Euler angle $\theta = 0$ degrees in the torque-free case no longer occurs since the Euler angle θ is bound between -45 and -90 degrees. The precession angle represents the change of angular momentum in the orbital coordinate system in the orbit normal-velocity vector plane. Examination of the gravity-gradient torque equations in the orbital coordinate system, equations (34), for a symmetric satellite about the minor axis ($B=C$) indicates why the regular precession occurs. Making the assumption ($B=C$) for Skylab the gravity-gradient torque equations in the orbital coordinate system become

$$\begin{aligned} (M_x)_o &= \sin 2\theta \sin \psi (A-C) 3\mu/2R^3 \\ (M_y)_o &= \sin 2\theta \cos \psi (C-A) 3\mu/2R^3 \\ (M_z)_o &= 0 \end{aligned} \quad (72)$$

M_x and M_y are the torque components in the orbit normal-velocity vector plane and are functions of θ and ψ . Since θ is bound between -40 and -90 degrees the Euler angle ψ controls the direction of the precession.

The nutation angle represents the motion of the angular momentum vector with respect to the orbit radius vector. Since the z gravity-gradient torque component in the orbital coordinate system is zero the

REPRODUCIBILITY OF THE
ORIGINAL PAGE IS POOR

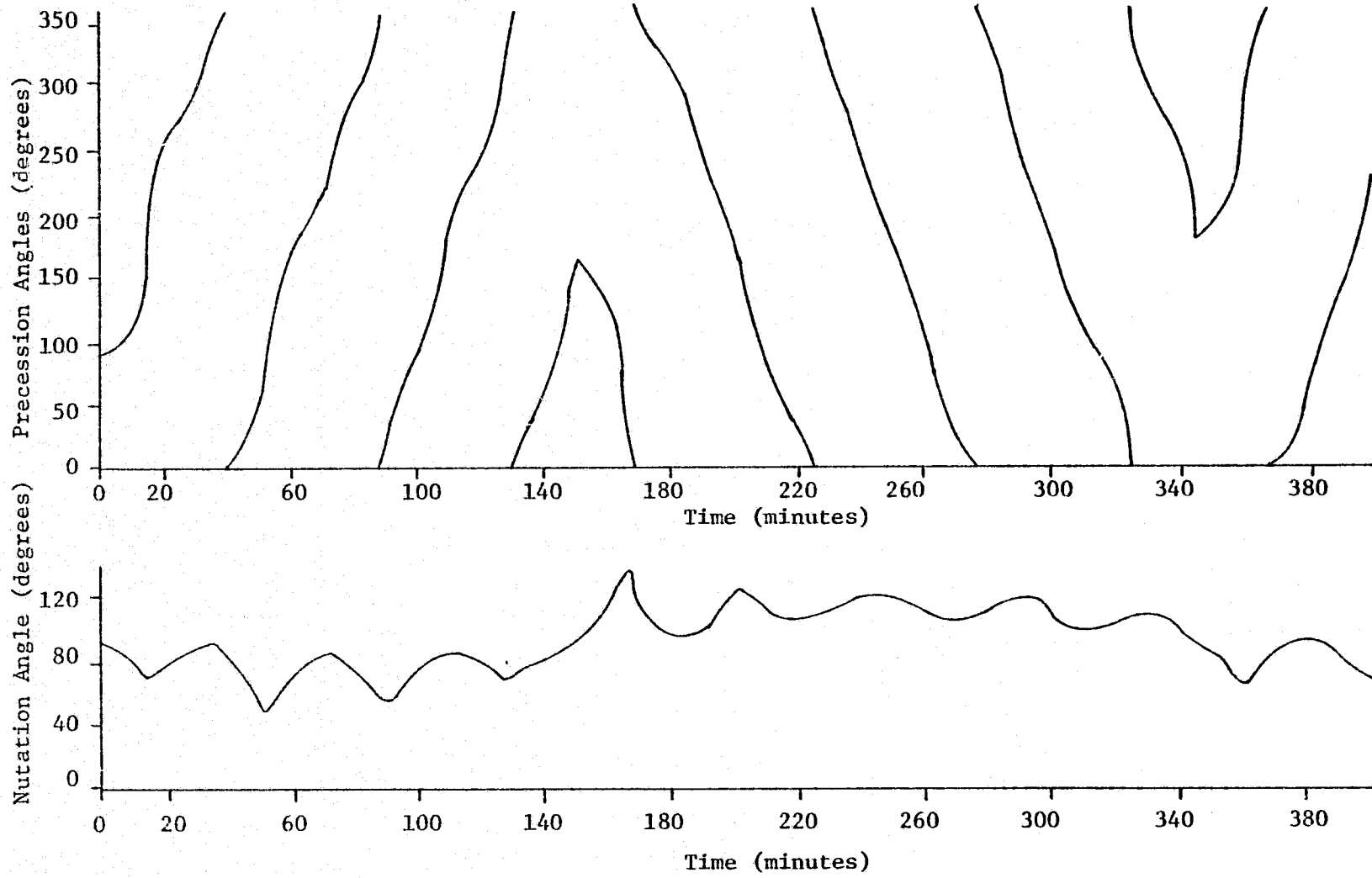


Figure 16. Nutation and Precession Angles for Gravity-Gradient.

the nutation angle reflects the change in the total angular momentum magnitude. The nutation angle is shown in Figure 16.

Gravity-gradient causes the angular momentum and energy to become cyclic, attempts to align the minor axis along the orbit radius vector, and causes a regular precession of the angular momentum about the orbit radius vector.

Aerodynamic Drag Results

The aerodynamic torque equations are complex and difficult to examine analytically. However, by examining the trends of various spacecraft attitude parameters, valuable insight into the problem can be gained.

Figure 17 illustrates the motion of the minor axis with respect to the orbit radius vector. As compared with the torque-free case, Figure 13, aerodynamic torques tend to damp out the oscillations and drive the minor axis perpendicular to the orbit radius vector. Since the free streamline velocity vector is approximately parallel to the orbit velocity vector, aerodynamic drag would orient the spacecraft toward a position of minimum resistance. From Figure 17 this position would appear to occur when the minor axis is in the orbit normal velocity vector plane. This can be illustrated by examining the nadir angle. The nadir angle amplitude continues to decrease in magnitude until 310 minutes and is oscillating about the velocity vector tangent (nadir angle of 90°).

Figure 18 illustrates the change in angular momentum and energy. As shown the angular momentum and energy decrease until approximately 310 minutes. After this time the angular momentum and energy begin to increase.

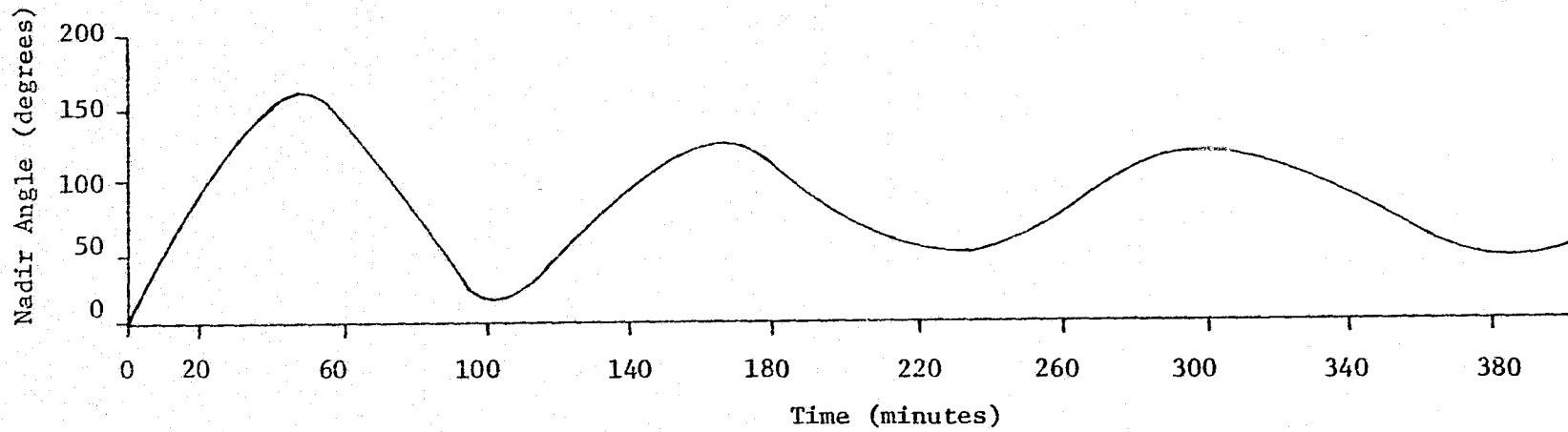


Figure 17. Nadir Angle for Aerodynamic Drag.

REPRODUCIBILITY OF THE ORIGINAL PAGE IS POOR

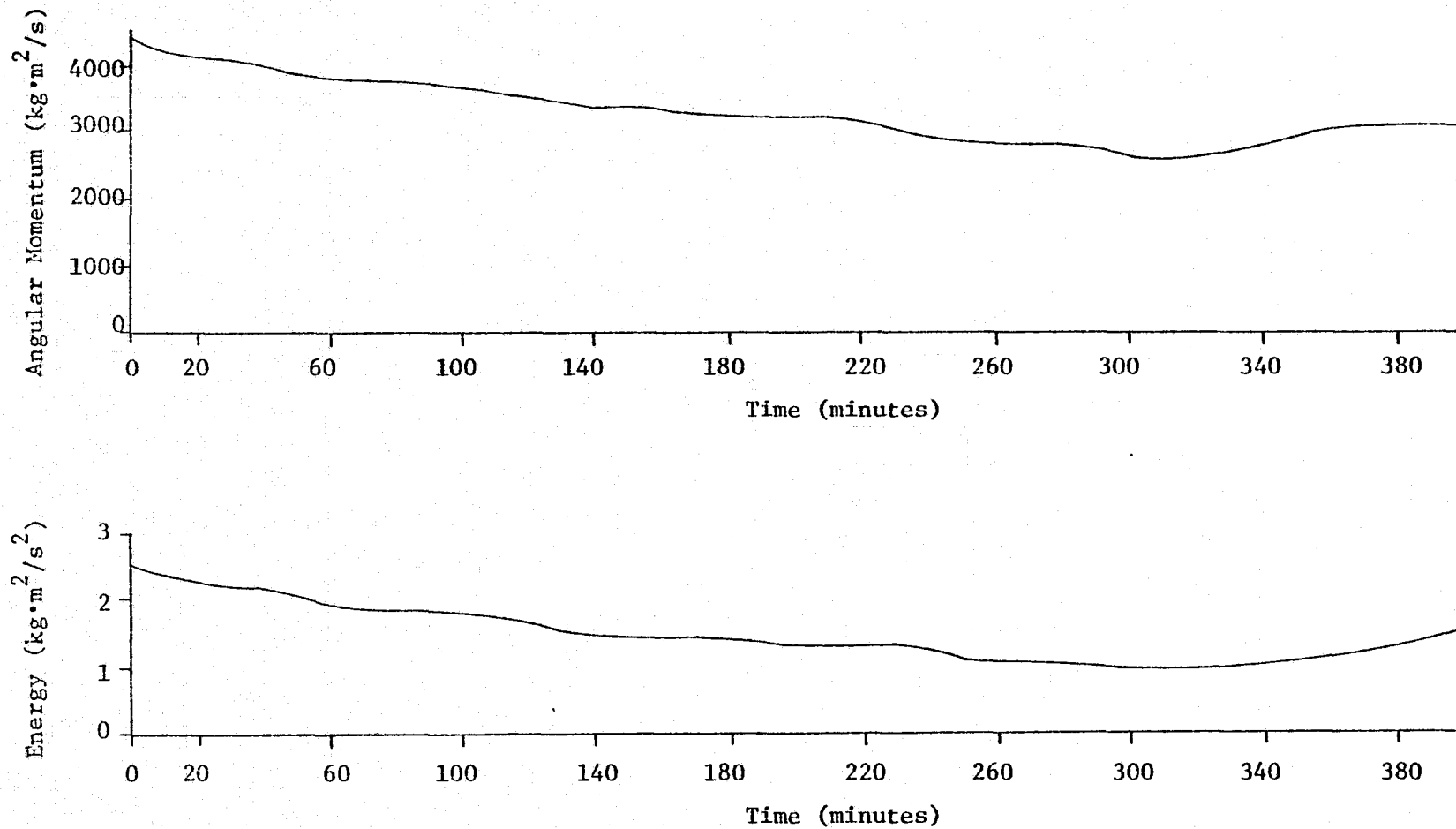


Figure 18. Aerodynamic Drag Effect on the Angular Momentum and Energy.

An explanation for the above trends can be found by examining the change in angular momentum in the spacecraft body coordinate system. Figure 19 illustrates the angular momentum change for the major axis (B) and the intermediate axis (C). The angular momentum change for the minor axis (A) was very small. As shown in Figure 19 initially the spacecraft was principally spinning about the major axis. As time progressed the aerodynamic effect caused the angular momentum to shift from the major axis to the intermediate axis until the spacecraft was essentially spinning about the intermediate axis at approximately 310 minutes. From attitude dynamics⁽⁵⁾ a spacecraft spinning about the intermediate axis with a perturbation is in an unstable mode. Reference 15 illustrates why an unstable mode exists for motion about the intermediate axis with a perturbation. After reaching this unstable mode the spacecraft quickly changes its momentum state and within an orbit is spinning about the major axis. It is interesting to note that the spacecraft is spinning about the major axis in the direction opposite to its initial one. This change in angular momentum state causes the nadir angle, angular momentum, and energy to increase.

The aerodynamic drag effect on the position of the angular momentum vector in the orbital coordinate system is illustrated in Figure 20. As compared to the torque-free solution, the oscillatory motion of the nutation angle is damped out and the momentum vector tends to align along the radius vector. The nutation angle continues to decrease until approximately 310 minutes. As the minor axis is being forced to become parallel to the orbit's velocity vector tangent the momentum is being transferred from the major to intermediate axis as shown in Figure 19 and explains the reason for the decrease. The

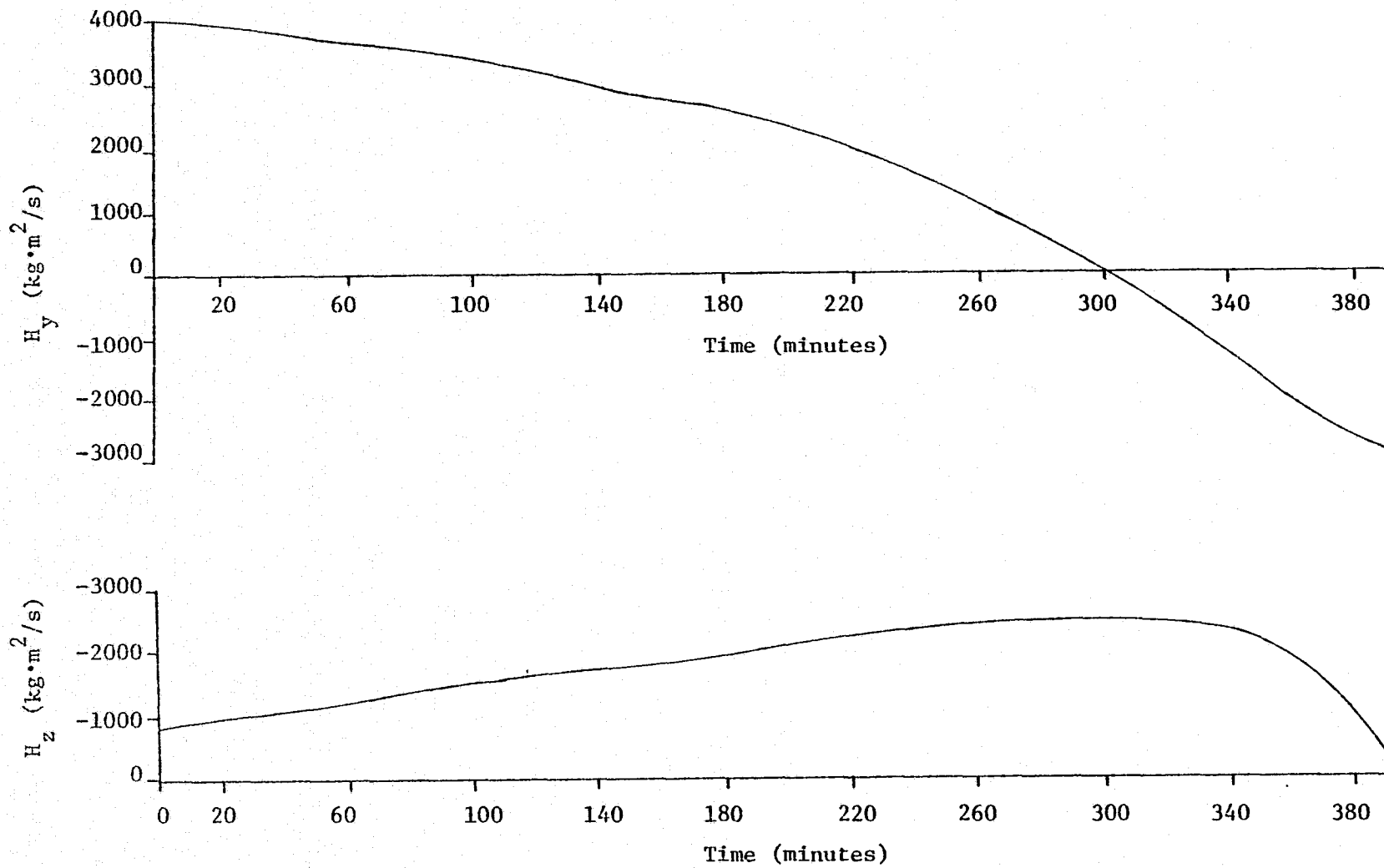


Figure 19. Effect of Aerodynamic Drag on the Y and Z Angular Momentum Components in the Body Coordinate System.

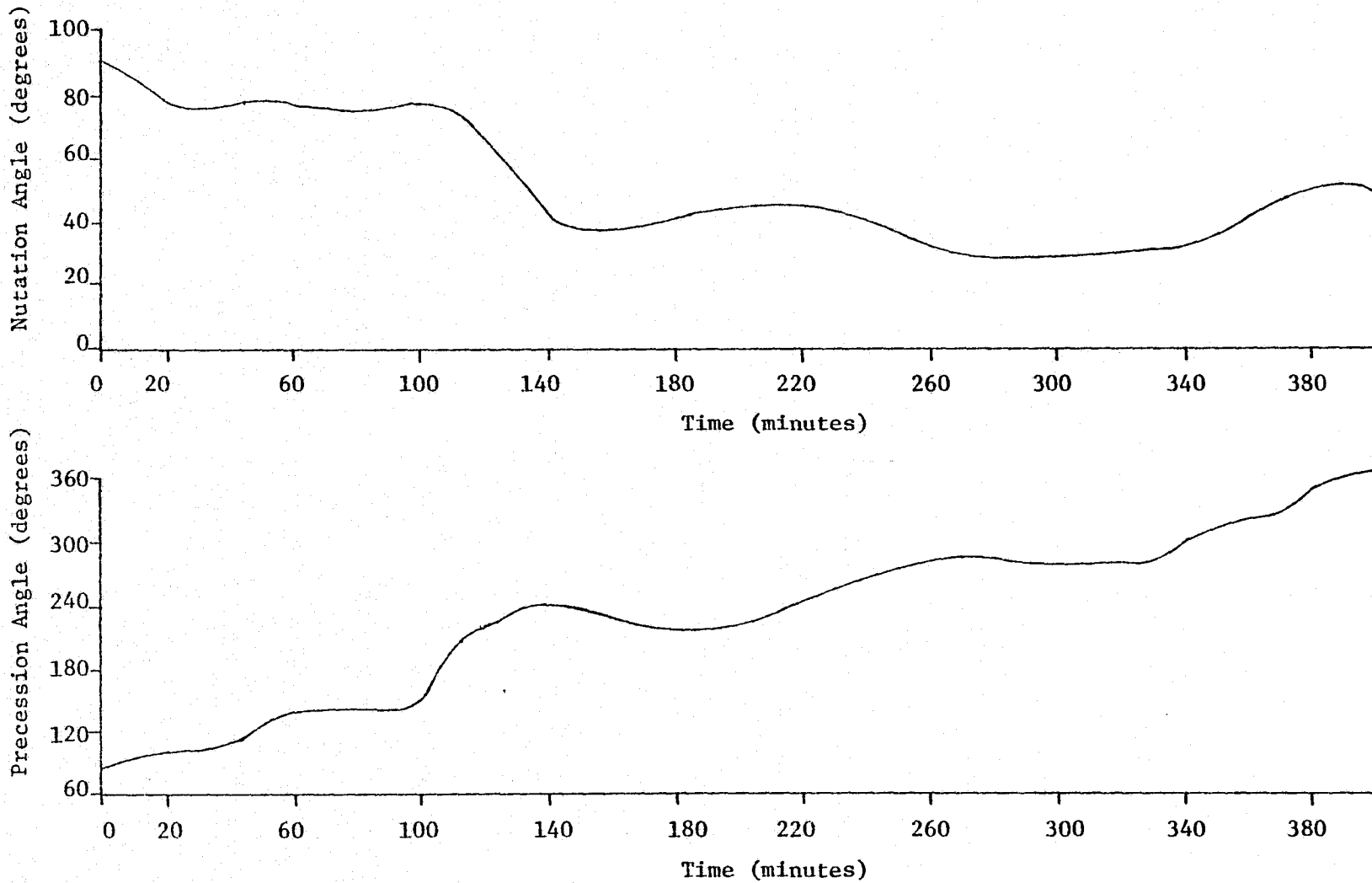


Figure 20. Aerodynamic Drag Effect on the Precession and Nutation Angles.

REPRODUCIBILITY OF THE
ORIGINAL DATA IS POOR

intermediate axis is oriented in the general direction of the orbit's radius vector. As a result the nutation angle decreases until the angular momentum is transferred back to the principal axis. As the angular momentum is transferred back to the major axis the nutation angle increases. The aerodynamic effect on the precession angle is to cause it to precess slowly about the orbit radius vector as shown in Figure 20.

Combined Effects of Gravity-Gradient and Aerodynamic Torques

The combined effect of aerodynamic and gravity-gradient torques on the energy and angular momentum is illustrated in Figure 21. Since gravity-gradient is larger than aerodynamic drag the cyclic motion due to gravity-gradient is predominant. The periodic type motion of the angular momentum and energy resulting from gravity-gradient becomes a random type oscillation due to the damping effect of aerodynamic drag. The aerodynamic torque reduces the amplitude of the gravity-gradient induced oscillations. Initially the amplitude of oscillations varied between 600 and 4200 $\text{kg}\cdot\text{m}^2/\text{s}$; as time progressed the amplitudes varied between 2700 and 4200 $\text{kg}\cdot\text{m}^2/\text{s}$. The lower limit of the gravity-gradient oscillation was affected more severely. This was due to the aerodynamic effect of aligning the minor axis along the velocity vector.

Comparing the nadir angle of gravity-gradient (Figure 14) and gravity-gradient with aerodynamic drag (Figure 21) illustrates the aerodynamic effect. Aerodynamic drag reduces the amplitude of oscillation of the angular momentum and nadir angle which were induced by the gravity-gradient torque. This torque tends to align the minor axis along the radius vector. The aerodynamic torque attempts to align the

REPRODUCIBILITY OF THE
ORIGINAL VALUE IS 20%

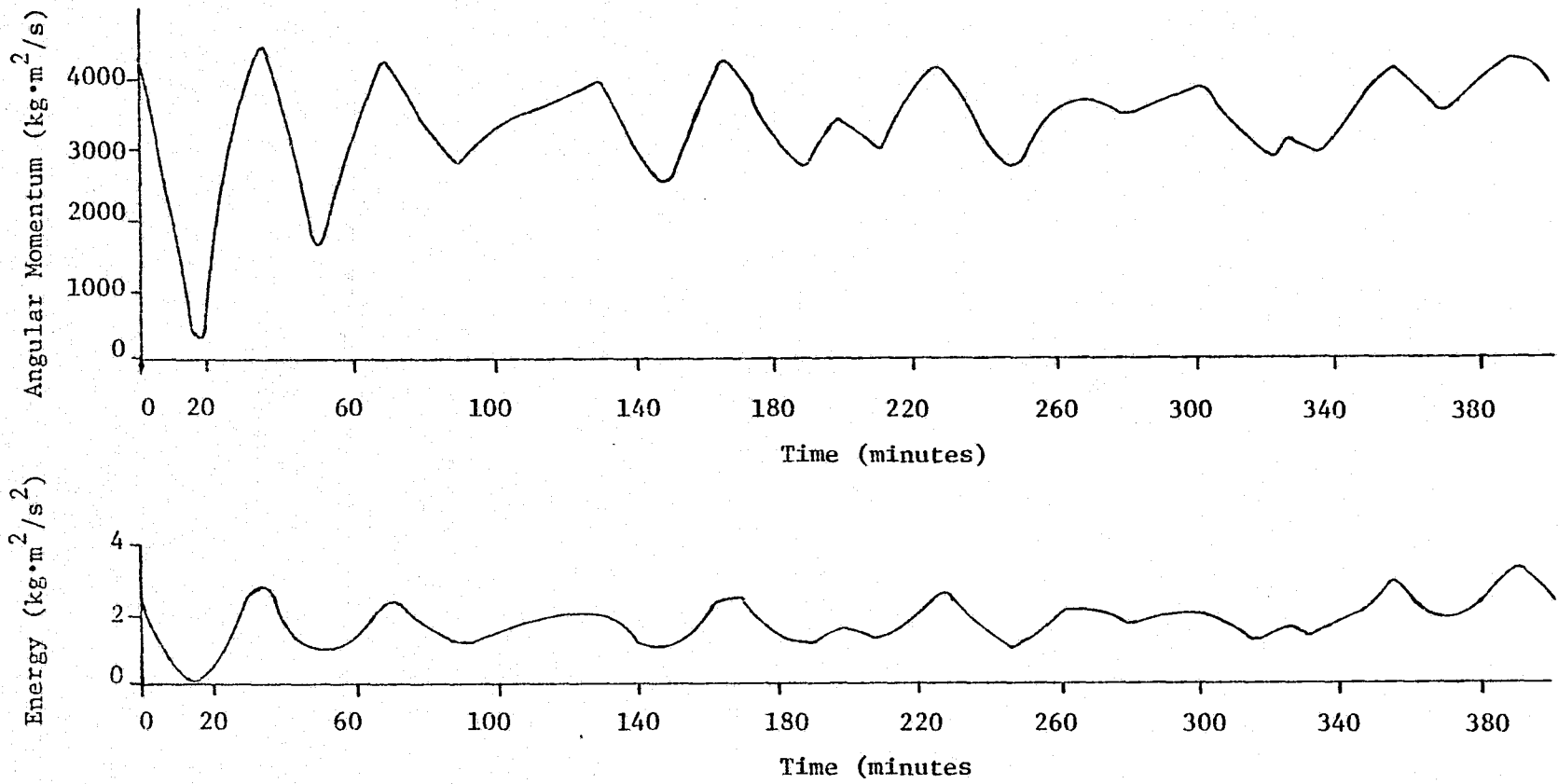


Figure 21. Aerodynamic Drag and Gravity-Gradient Effect on the Angular Momentum and Energy.

minor axis along the orbit velocity vector tangent perpendicular to the orbit radius. The combined effect of gravity-gradient and aerodynamic torque is to cause the minor axis to oscillate between the radius vector and orbit velocity vector tangent as illustrated in Figure 22. Since the gravity-gradient torque is larger than aerodynamic, its effect is predominant. This causes the minor axis to oscillate nearer the orbit radius vector between 25 and 30 degrees.

Since the gravity-gradient torque component in the orbit radius vector is zero the change in nutation angle illustrated in Figure 23 is due to the aerodynamic torque. The effect of the aerodynamic torque is to maintain the angular momentum vector below the orbit velocity vector-orbit normal plane. The precession angle as shown in Figure 23 has a period of approximately 46 minutes. This is similar to gravity-gradient effect shown in Figure 14. The difference is aerodynamic torque eliminates the change in the precession angle direction. As a result the combined effect of gravity-gradient torque with aerodynamic drag is to cause the angular momentum vector to precess regularly about orbit radius vector pointing down the radius vector.

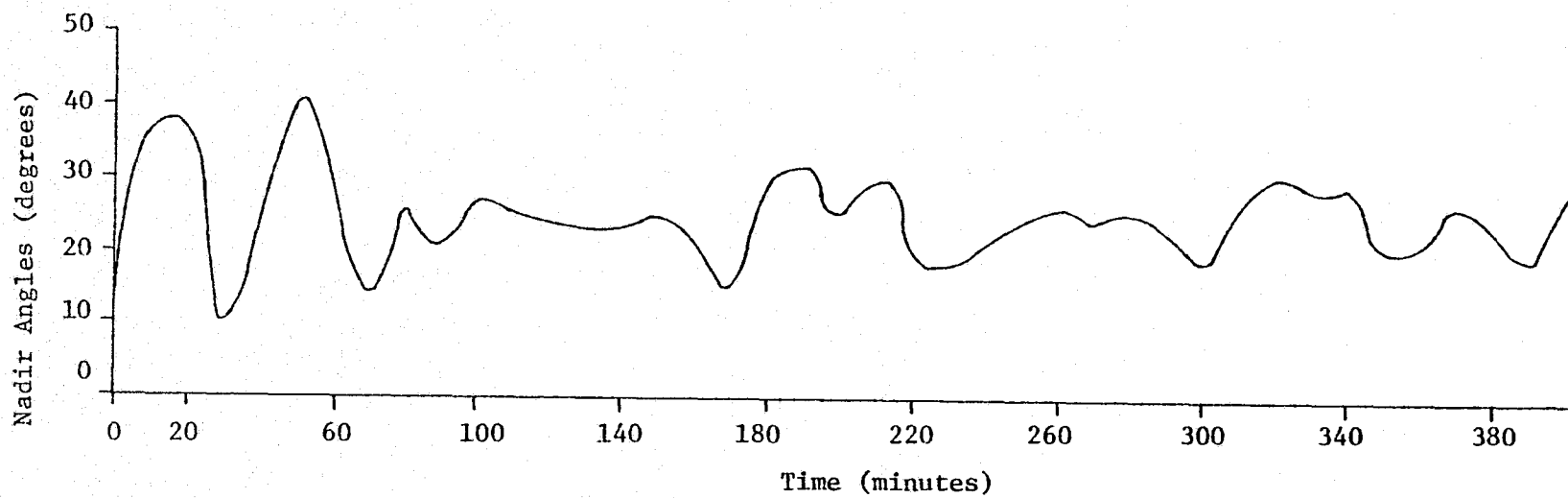


Figure 22. Nadir Angle for Aerodynamic Drag and Gravity-Gradient.

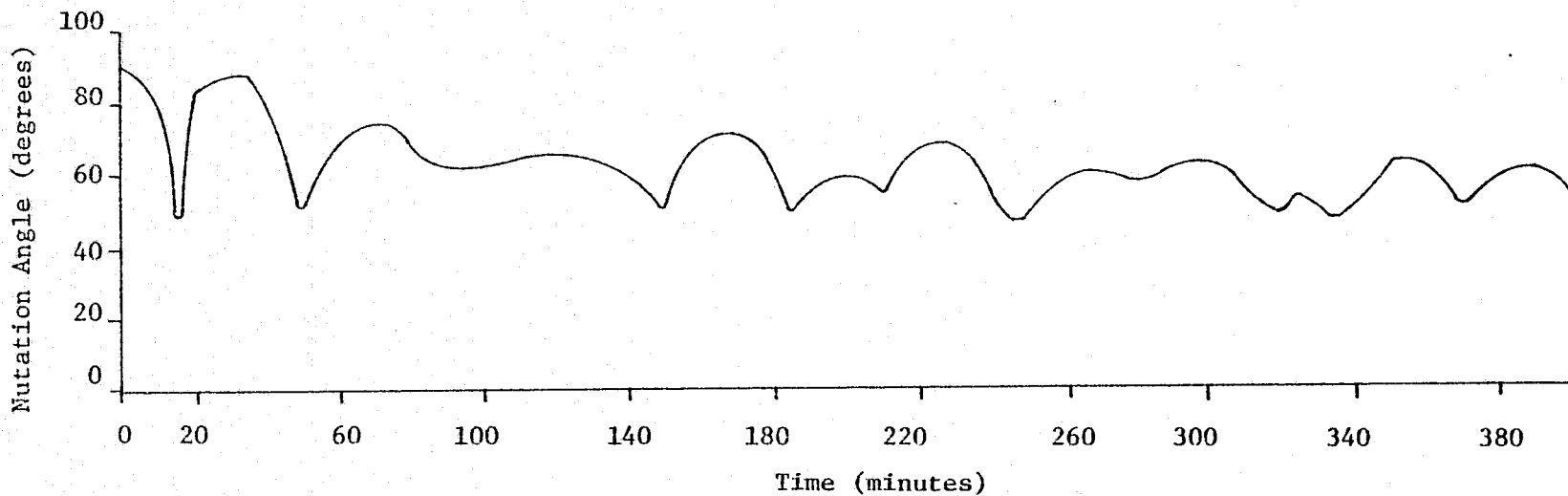
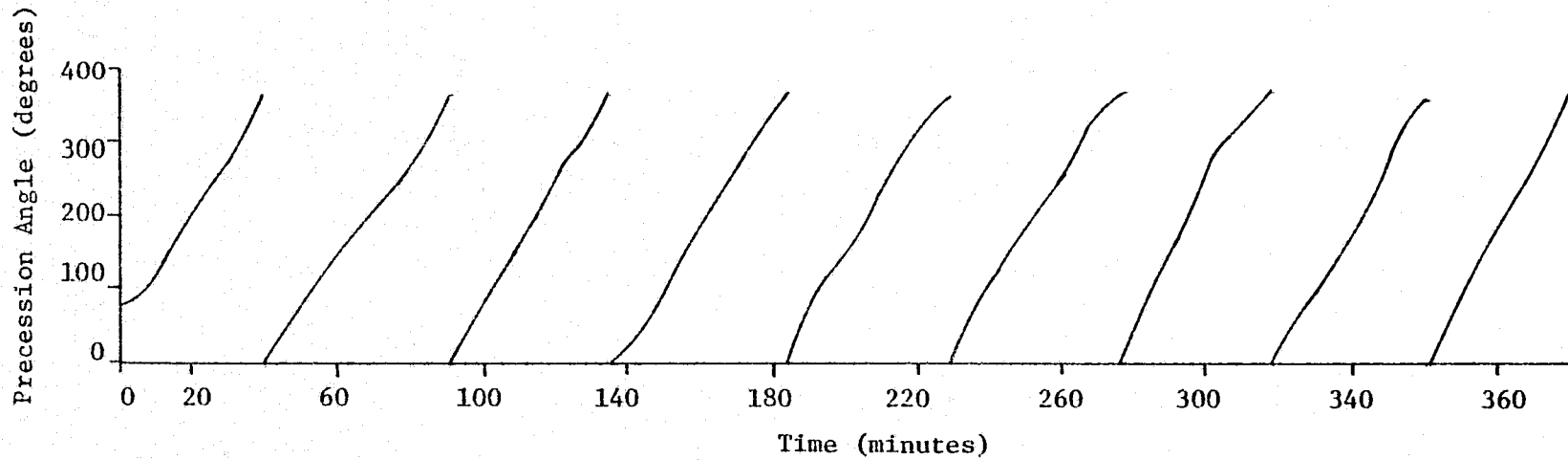


Figure 23. Aerodynamic Drag and Gravity-Gradient Effect on the Precession and Nutation Angles.

REPRODUCTION OF THIS
 DOCUMENT IS UNLIMITED

CHAPTER VII

CONCLUSIONS AND RECOMMENDATIONS

An investigation of environmental perturbations for an asymmetric slow tumbling satellite has been presented. Environmental perturbation sources considered were gravity-gradient, aerodynamic drag, solar radiation pressure and magnetic field interactions. For the Skylab spacecraft results assuming gravity-gradient and aerodynamic torques were presented. Solar radiation pressure and magnetic torques were small and neglected.

Gravity-gradient torque causes the nadir angle to become bounded about the orbit radius vector and causes the energy, angular momentum, and precession angle to become cyclic. Aerodynamic drag initially decreased the angular momentum, energy, and nadir angle and drives the spacecraft into an unstable mode by transferring angular momentum from the major axis to the intermediate axis. Aerodynamic drag also induces slow precession rate about the orbit radius vector and causes the nutation angle to decrease. The combined effects of gravity-gradient with aerodynamic torques were to cause the gravity-gradient induced oscillation amplitudes to decrease and the periodic motion to become random type oscillations. Gravity-gradient torques were greater than aerodynamic drag and its effect was predominant.

For long term predictions of satellite tumbling motion, analytical techniques must be investigated. Computer simulation for this type of motion becomes very expensive since small time intervals are required to solve the nonlinear equations of motion. Future models of tumbling

spacecraft should include energy dissipation models to account for internal energy dissipation.

REFERENCES

1. Thompson, W. T., Introduction to Space Dynamics, John Wiley and Sons, Inc., New York, 1963, pp. 111-113.
2. Frik, M. A., "Attitude Stability of Satellites Subjected to Gravity Gradient and Aerodynamic Torques," NASA TM X-53796, October 1968.
3. Nurre, G. S., "Attitude Dynamics of the S-IVB Orbital Workshop Influenced by Gravitational and Aerodynamic Torques," NASA TM X-53691, January 1968.
4. Nurre, G. S., "Effects of Aerodynamic Torque on an Asymmetric, Gravity-Stabilized Satellite," NASA TM X-53688, January 1968.
5. Palmer, J. L., "Generalized Spacecraft Simulation," TRW Report 064640600-TC0, February 1967, pp. 9-2 - 9-15.
6. Greensite, A. L., "Attitude Control in Space," Analysis and Design of Space Vehicle Flight Control Systems, Vol. XII, NASA, CR-831, Washington, D. C., August 1967, pp. 64-68.
7. Barnum, P. M., Firechsel, P. G., and Grunberger, P. J., "The Attitude Motion of a Nutationally Damped Dual-Spin Spacecraft in the Presence of Near Earth Environment," AIAA Paper No. 71-90, presented at the 9th Aerospace Sciences Meeting, New York, N. Y., January 1971.
8. Chambre, P. L., and Schaaf, S. A., Flow of Rarefied Gases, Princeton University Press, Princeton, New Jersey, 1961.
9. _____, "Skylab-I Performance Data," NASA-MS-01549, Vol. 4, October 1972, pp. 9-53, 55, C-1, C-25.
10. Lewis, J. R., "RTCC and MOPS Requirements for Modified 1970 Jacchia Atmosphere Model," NASA MSC Internal Note No. 70-FM-202, January 1971.
11. Cain, J. C., and Cain, S. J., "Computation of the Main Geomagnetic Field from Spherical Harmonic Expansions," NASA-NSSDC 68-11, May 1968.
12. Cain, J. C., and Cain, S. J., "Derivation of the International Geomagnetic Reference Field," NASA TN D-6237, August 1971.
13. Clancy, T. F., and Mitchell, T. P., "Effects of Radiation Force on the Attitude of an Artificial Earth Satellite," AIAA Journal, No. 3, Vol. 2, 1964, pp. 517-524.

REFERENCES (continued)

14. Beckett, R., and Hurt, J., Numerical Calculations and Algorithms, John Wiley and Sons, Inc., New York, 1967, pp. 192-220.
15. Kaplan, M. H., Modern Spacecraft Dynamics and Control, John Wiley and Sons, Inc., New York, pp. 68-72; (to be published in 1976).

APPENDIX A

Initial Conditions for the Slow Tumble Mode

A. Slow Tumble Orientation

The Skylab spacecraft was assumed to be in the following attitude

$$\psi = 1.07 \text{ degrees}$$

$$\theta = -79.96 \text{ degrees}$$

$$\phi = 12.85 \text{ degrees}$$

This was the attitude Skylab was believed to be in when it became passive. For the slow spin case a negative angular velocity equal in magnitude to the orbital rate about the orbit normal was assumed.

$$\omega_o = +.00112256 \text{ radians/second}$$

$$\bar{\omega}_o = \omega_o \bar{j}_o$$

Using the transformations and Figure (4) the required initial Euler rates can be computed.

$$\dot{\psi} = 0.0$$

$$\dot{\theta} = \omega_o \cos \psi$$

$$\dot{\phi} = \omega_o \sin \psi \cos \theta$$

Assuming ω_o is the negative of the orbital rate the initial Euler rates for the flow tumble case are

$$\dot{\psi} = 0.0$$

$$\dot{\theta} = -.0011229 \text{ radians/second}$$

$$\dot{\phi} = -3.656 \times 10^{-6} \text{ radians/second}$$

APPENDIX B

Skylab's Aerodynamic Drag Moment Coefficients

	a_0	a_1	a_2	a_3	a_4	a_4	a_6
	b_1	b_2	b_3	b_4	b_5	b_6	
	c_y (pitching moment coefficient)						
A ₁	-1.289	0.135	-0.195	-0.009	0.080	0.007	-0.037
A ₁	-0.004	0.009	-0.011	0.022	-0.005	0.011	
A ₃	0.442	-0.073	0.084	0.000	-0.076	-0.011	0.003
A ₃	0.009	-0.022	0.015	-0.036	0.007	-0.020	
B ₁	-0.037	-5.146	0.011	0.350	0.014	-0.010	-0.007
B ₁	0.199	-0.017	0.120	0.002	-0.06	0.009	
B ₃	-0.044	0.779	-0.007	0.123	0.005	-0.032	-0.001
B ₃	-0.049	-0.012	-0.021	0.001	0.032	-0.001	
	c_z (yawing moment coefficient)						
A ₁	-0.958	-0.067	-0.266	0.019	0.016	-0.006	0.012
A ₁	-0.096	-0.055	-0.026	-0.054	0.018	-0.009	
A ₃	0.269	0.006	0.207	-0.007	-0.032	0.006	-0.014
A ₃	0.055	0.031	0.014	0.068	-0.027	0.012	
B ₁	0.166	-0.140	-0.014	0.280	-0.042	-0.074	0.046
B ₁	4.210	0.022	0.454	-0.052	-0.055	0.003	
B ₃	0.155	0.072	0.003	-0.069	-0.015	-0.032	0.004
B ₃	-0.467	0.004	-0.134	-0.010	0.003	-0.001	
	c_x (rolling moment coefficient)						
A ₁	-0.056	-0.071	-0.038	0.009	-0.012	-0.001	0.006
A ₁	0.018	-0.035	0.013	-0.017	0.002	-0.011	
A ₃	0.078	0.047	0.058	-0.009	0.018	0.005	-0.016
A ₃	-0.021	0.042	-0.016	0.028	-0.000	0.018	
B ₁	0.053	1.136	0.024	0.250	-0.005	-0.039	-0.007
B ₁	0.943	-0.016	0.430	0.005	-0.052	-0.005	
B ₃	0.025	-0.210	0.009	-0.055	-0.005	0.019	-0.003
B ₃	-0.162	0.005	-0.099	0.000	0.007	-0.002	

REPRODUCIBILITY OF THE
ORIGINAL PAGE IS POOR

APPENDIX C

Skylab's Orbit and Satellite Parameters

Orbital Parameters

Orbit Inclination = 50 degrees

Eccentricity = 0

Altitude = 435.5 kilometers

Right Ascension of Ascending Node = 233.2 degrees

Orbital Period = 93.23 minutes

Earth's gravitational constant = 3.986×10^5 kilometer³/second²

Earth's mean radius - 6378.0 kilometers

Satellite Parameters

Principal Moment of Inertias

$$I_{xx} = 7.93321 \times 10^5 \text{ kilograms - meter }^2$$

$$I_{yy} = 3.767828 \times 10^6 \text{ kilograms - meter }^2$$

$$I_{zz} = 3.694680 \times 10^6 \text{ kilograms - meter }^2$$

Aerodynamic Reference Area

$$\text{Surface Reference Area} = 79.46 \text{ meter}^2$$

$$\text{Reference Diameter} = 10.058 \text{ meter}$$